

# The False Promise of Zero-Shot Super-Resolution in Machine-Learned Operators

Mansi Sakarvadia<sup>1\*</sup>, Kareem Hegazy<sup>5,6</sup>, Amin Totounferoush<sup>3</sup>, Kyle Chard<sup>1</sup>  
Yaoqing Yang<sup>4</sup>, Ian Foster<sup>1</sup>, Michael W. Mahoney<sup>2,5,6</sup>

<sup>1</sup>University of Chicago, <sup>2</sup>Lawrence Berkeley National Laboratory, <sup>3</sup>University of Stuttgart,  
<sup>4</sup>Dartmouth College, <sup>5</sup>International Computer Science Institute, <sup>6</sup>University of California, Berkeley

## Abstract

A core challenge in scientific machine learning, and scientific computing more generally, is modeling continuous phenomena which (in practice) are represented discretely. Machine-learned operators (MLOs) have been introduced as a means to achieve this modeling goal, as this class of architecture can perform inference at arbitrary resolution. In this work, we evaluate whether this architectural innovation is sufficient to perform “zero-shot super-resolution,” namely to enable a model to serve inference on higher-resolution data than that on which it was originally trained. We comprehensively evaluate both zero-shot sub-resolution *and* super-resolution (i.e., multi-resolution) inference in MLOs. We decouple multi-resolution inference into two key behaviors: 1) extrapolation to varying frequency information; and 2) interpolating across varying resolutions. We empirically demonstrate that MLOs fail to do both of these tasks in a zero-shot manner. Consequently, we find MLOs are *not* able to perform accurate inference at resolutions different from those on which they were trained, and instead they are brittle and susceptible to aliasing. To address these failure modes, we propose a simple, computationally-efficient, and data-driven multi-resolution training protocol that overcomes aliasing and that provides robust multi-resolution generalization.

## 1 Introduction

Modeling physical systems governed by partial differential equations (PDEs) is critical to many computational science workflows:

$$S_2 = M(S_1), \quad (1)$$

where  $M$  is an approximation of the PDE’s solution operator,  $S_1$  is the input state of the system, and  $S_2$  is the predicted state. Central to this problem formulation is that *continuous* physical systems must be sampled and, therefore, modeled *discretely*. For a discrete model,  $M$ , to be useful in representing phenomena of different scales, scientists require the ability to use it at different resolutions accurately. For example, when modeling fluid flow, scientists often use adaptive mesh refinement (Berger & Olinger, 1984), a technique that increases simulation resolution in areas that require high accuracy (e.g., regions of turbulence), and coarsens the resolution in less critical regions.

Traditionally, the approximation  $M$  is constructed by numerical methods which, by design, can be employed at arbitrary discretization (Forrester et al., 2008; Cozad et al., 2014; Asher et al., 2015; Sudret et al., 2017; Alizadeh et al., 2020; Kudela & Matousek, 2022). However, numerical methods are computationally expensive. Alternatively, machine-learned operators (MLOs), a class of data-driven machine learning (ML) models which parameterize the solution operator to families of PDEs, have been proposed (Raissi et al., 2019; Li et al., 2020a; Lu et al., 2021; Kovachki et al., 2023; Raonic et al., 2023). Although querying MLOs at arbitrary discretization is computationally inexpensive, it is not obvious that this can be done *accurately*. The Fourier Neural Operator (FNO) (Li et al., 2020a), a specific MLO, claimed to address the discretization challenge in a *zero-shot* manner (Li et al., 2020a; Tran et al., 2021; George et al., 2024; Li et al., 2024b; Azzizadenesheli et al., 2024). The claim is that an FNO can be trained at resolution  $m$  and can then serve accurate inference<sup>3</sup> at resolution  $n > m$ , without training on additional high resolution data. In machine learning terminology, this is *zero-shot super-resolution*. This claim of zero-shot super-resolution, if true, would be especially attractive in settings where generating, and training on, high-resolution data is computationally expensive.

\*Correspondence to [sakarvadia@uchicago.edu](mailto:sakarvadia@uchicago.edu), Code: [https://github.com/msakarvadia/operator\\_aliasing](https://github.com/msakarvadia/operator_aliasing)

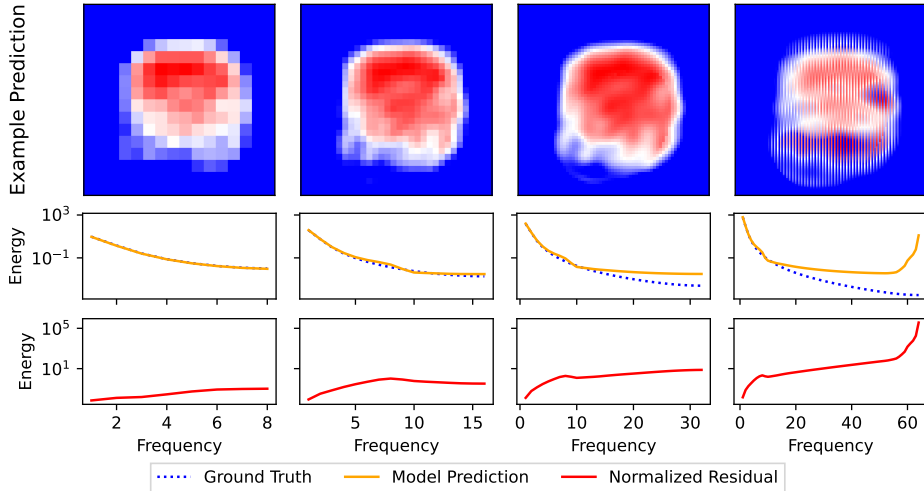


Figure 1: **Aliasing in zero-shot super-resolution.** Model trained on resolution 16 data, and evaluated at varying resolutions: 16, 32, 64, 128. **Top Row:** Sample prediction for Darcy flow; notice striation artifacts at resolution 128. **Middle Row:** Average test set 2D energy spectrum of label and model prediction. **Bottom Row:** Average residual spectrum normalized by label spectrum.

In this paper, we evaluate the claim of zero-shot super- (and sub-)resolution inference in MLOs. We document a substantial disparity in model performance across data of different discretizations, suggesting that MLOs are generally incapable of accurate inference at resolutions greater than, or less than, their training resolution (i.e., zero-shot multi-resolution inference). Instead, we find that MLOs often misrepresent unseen frequencies and incorrectly infer their behavior in data whose discretization differs from its training discretization, i.e., they exhibit a form of aliasing (see Fig. 1). In addition, we study two previously proposed solutions: (i) physics-informed optimization constraints (Li et al., 2024b); and (ii) band-limited learning (Raonic et al., 2023; Gao et al., 2025). We find that neither enables zero-shot multi-resolution, as they do *not* address the central issue: MLOs, like all machine-learned models, cannot typically generalize beyond their training data (Yang et al., 2023; Liu et al., 2020; Krueger et al., 2021); and changing the discretization of test data constitutes a (specific) form of out-of-distribution inference. We establish that the discretization at which MLOs are trained impacts the discretization at which they *accurately* model the system.

To enable multi-resolution inference, we propose *multi-resolution training*, a simple, intuitive, and principled data-driven approach which trains models on data of multiple resolutions. We profile the impact of different multi-resolution training approaches, finding that optimal multi-resolution performance can often be achieved via training data sets that contain mostly low resolution (less expensive) data and very little high resolution (more expensive) data. This permits us to achieve low computational overhead, while also increasing the utility of a single MLO.

To summarize, the main contributions of our work are the following:

1. We assess the ability of trained MLOs to generalize beyond their training resolution. We demonstrate that MLOs struggle to perform accurate inference at resolutions higher than or lower than the resolution on which they were trained, and instead exhibit a form of aliasing. Based on these results, we conclude that accurate *zero-shot* multi-resolution inference is brittle and unreliable. (See Sec. 3.)
2. We evaluate two intuitive approaches—incorporating physics-informed constraints during training, as well as performing band-limited learning—and we find that neither approach enables reliable multi-resolution generalization. (See Sec. 4.)
3. We propose and test multi-resolution training, where we include training data of varying resolutions (in particular, a small amount of expensive higher-resolution data and a larger amount of cheaper lower-resolution data), and we show that multi-resolution inference improves substantially, without a significant increase in training cost. (See Sec. 5.)

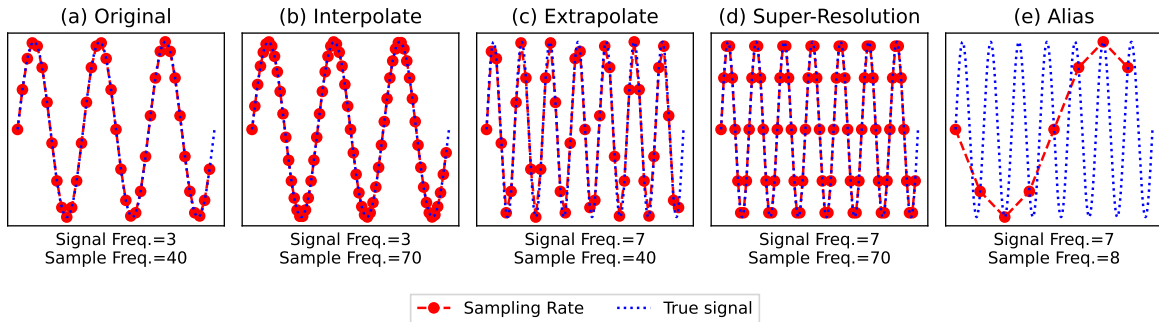


Figure 2: **Accurate multi-resolution inference requires both interpolation and extrapolation.** **Original:** Signal is sampled at a rate greater than its Nyquist frequency. **Interpolation:** Adapting to new sampling rates of a given signal. **Extrapolation:** Adapting to new frequency information under constant sampling rate. **Super-Resolution:** Sampling a system at a higher rate, which enables the capture of higher frequency information (interpolation and extrapolation). **Aliasing:** High-frequency information is misrepresented as a low-frequency information due to insufficient sampling.

## 2 Background on Signal Processing and Aliasing

We start by discussing the practice of training ML models to represent continuous systems via discrete data. Then, we outline the implications of aliasing in ML as it relates to multi-resolution inference. Finally, we formally define “zero shot multi-resolution” inference in a discrete context.

**Discrete Representations of Continuous Systems.** The fundamental challenge in discretely representing continuous systems lies in the choice of sampling rate. The Whittaker–Nyquist–Shannon sampling theorem established that, given a sampling rate  $r$ , the largest resolved frequency is  $r/2$  (Unser, 2002; Shannon, 1949; Whittaker, 1928). Thus, ML models will be trained on discrete representations, where only some of the frequencies are fully resolved. Resolving higher-order frequencies greater than  $r/2$ , consequently, becomes an out-of-distribution task. Aligning these discrete models’ predictions with the underlying continuous system is a non-trivial open problem (Krishnapriyan et al., 2021; Queiruga et al., 2020; Ott et al., 2021; Ren et al., 2023; Takamoto et al., 2022; Subel et al., 2022; Chattopadhyay et al., 2024).

**Aliasing.** When sampling a continuous signal at rate  $r$ , aliasing occurs when frequency components greater than  $r/2$  are projected onto lower frequency basis functions (see Fig. 2) (Gruver et al., 2022). When this happens, content with frequency  $n > r/2$  is observed as a lower frequency contribution:

$$\text{Alias}(n) = \begin{cases} n \bmod r & \text{if } (n \bmod r) < r/2 \\ r - (n \bmod r) & \text{if } (n \bmod r) > r/2 \end{cases} \quad (2)$$

Within an ML context, when inferring at different discretizations of a given signal, aliasing can manifest as the divergence between the energy spectrum of the model prediction and the expected output. Aliasing indicates a model’s failure to fit the underlying continuous system.

**Zero-shot multi-resolution inference.** We define *multi-resolution* inference as the ability to do inference at multiple resolutions (e.g., sub-resolution *and* super-resolution). The *zero-shot* multi-resolution task employs an ML model, which is trained on data with some resolution, and then tested on data with a different resolution. Zero-shot multi-resolution inference raises two important questions with respect to the generalization abilities of trained models (see Fig. 2):

1. **Resolution Interpolation.** How do models behave when the frequency information in the data remains fixed, but its sampling rate changes from training to inference? Can the model *interpolate* the fully-resolved signal to varying resolutions?
2. **Information Extrapolation.** How do models behave when the resolution remains fixed, but the number of fully resolved frequency components changes from training to inference? For super-resolution, this means can the model *extrapolate* beyond the frequencies in its training data and model higher frequency information?

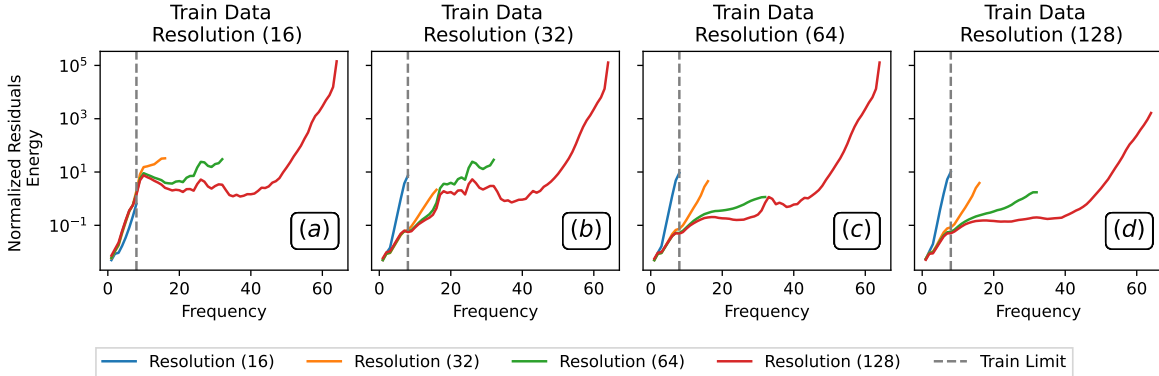


Figure 3: **Resolution Interpolation.** Four FNOs are trained on Darcy data at resolutions  $\{16, 32, 64, 128\}$  from left to right with constant frequency information (low-pass limit of  $8f$ ). We test whether each model can generalize to data with varying resolution, visualizing the normalized spectra of the residuals averaged across test data. Notice that the residual spectra (error) increases substantially in the higher frequencies. (Lower residual energy at all frequencies is better.)

### 3 Assessing Multi-Resolution Generalization

In this section, we examine the zero-shot multi-resolution abilities of FNO, an architecture for which this claim has previously been made (Li et al., 2020a). We study the multi-resolution inference task from an out-of-distribution data perspective by decoupling what it means for a model to perform inference at a resolution different from that used during training. Specifically, in Sec. 3.1, we assess whether models trained on a system sampled at rate  $r$  are capable of both interpolating accurately to **new** sampling rates (Fig. 2(b)) and extrapolating accurately to **additional/fewer** frequencies present in data (Fig. 2(c)). We systematically test an FNO’s ability to do both objectives and show neither are achieved. In light of these failure modes, in Sec. 3.2, we then assess the spatial zero-shot sub- and super-resolution capabilities of FNOs, and we show the claim does not hold (Fig. 2(d)).

We evaluate FNO on three standard scientific datasets: Darcy, Burgers, and Navier Stokes described in Appendix A. For each dataset we optimize FNO hyperparameters via grid-search as described in Appendix B.

#### 3.1 Breaking Down Multi-Resolution Capabilities

**Resolution Interpolation.** We assess whether an FNO trained on data of a specific resolution can generalize to data of both lower and higher resolution, under fixed frequency information. Specifically, we keep the set of populated frequencies constant in the train and test data, while varying the resolution of the test data. We do this by applying a low-pass filter to all data at the highest resolution, and then down-sampling as needed. The sampling rates of all data are large enough to resolve all remaining frequencies.

We begin with a simple experiment: we train an FNO on a Darcy flow dataset at resolution  $N = 16$  and assess the trained model’s performance across test datasets at varying resolutions  $\{16, 32, 64, 128\}$ , all low-pass filtered with limit  $8f$ , where  $f$  is the frequency unit  $2\pi/N$ . In Fig. 3(a), we visualize the average spectral energy of the model predictions, normalized by the spectral energy of the unfiltered ground truth for each test dataset. For the test data with resolutions that are different from the training data, we observe sharp increases in their residual’s energy spectrum in frequencies greater than  $8f$ . This is especially concerning since the model was never trained on nor shown inference data containing frequencies greater than  $8f$ . In other words, FNOs, trained in a zero-shot manner, fail to reliably *interpolate* to varying resolutions.

In Figs. 3(b-d), we repeat the same experiment at varying training resolutions (e.g. 32, 64, 128), with low-pass limit  $8f$ . We notice that at each training resolution, the model consistently and incorrectly assigns high energy in frequencies greater than  $8f$  across all test resolutions. We perform corresponding experiments for the Burgers dataset with low-pass limit  $64f$  and resolutions  $\in \{128, 256, 512, 1024\}$  and Navier Stokes dataset with low-pass limit  $32f$  and resolutions  $\in \{64, 128, 255, 510\}$  and observe

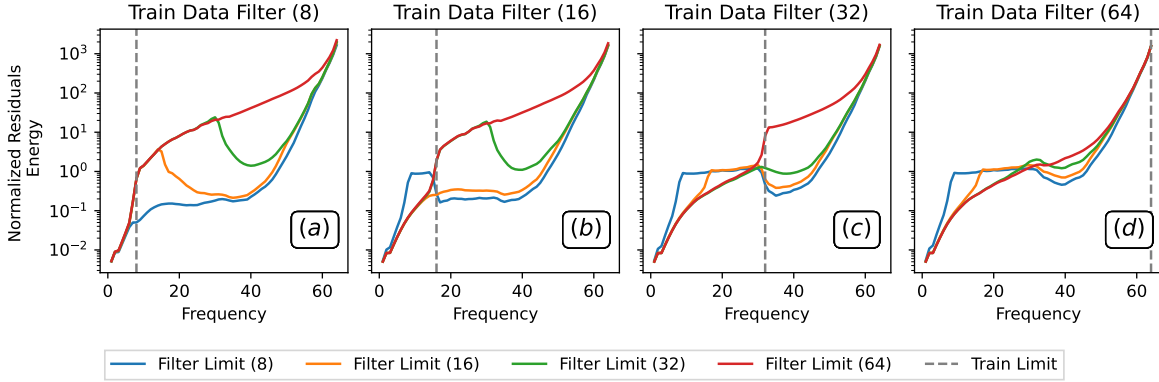


Figure 4: **Information Extrapolation.** Four FNOs trained on Darcy data of resolution 128 (constant sampling rate) and low-pass filtered with limits  $\{8, 16, 32, 64\}f$  (varying frequency information) from left to right. We test whether each model can generalize to data with varying frequency information, visualizing the normalized spectra of the residuals averaged across test data. Notice that the residual spectra (error) increases substantially in the higher frequencies. (Lower residual energy at all frequencies is better.)

the same failure mode (see Appendix C: Figs. 11-12). **We conclude that changing resolution at test time is akin to out-of-distribution inference:** the model is never trained on data with a broad range of sampling rates, and consequently, it fails to generalize.

**Information Extrapolation.** We assess whether an FNO trained on data containing a fixed set of frequencies can generalize to data containing both fewer and additional frequencies, under fixed resolution. Specifically, we keep the resolution constant but vary the number of populated frequencies in the train and test datasets by applying varying low-pass filters to data at a fixed resolution.

We begin with a simple experiment: an FNO is trained on a Darcy flow dataset at resolution 128 which is low-pass filtered at limit  $8f$ . In Fig. 4(a), we assess the trained model’s performance across four versions of a test dataset, all of which have the same sampling resolution (128) but are filtered with low-pass limits  $\{8, 16, 32, 64\}f$  (e.g., increasing amounts of frequency information). There is a sharp increase in the residual spectra in higher frequencies across all test sets; the residual error increases as the test and training filters diverge. In other words, FNOs, trained in a zero-shot manner, fail to *extrapolate* on data with previously unseen frequency information.

In Figs. 4(b-d), we repeat the same experiment at varying training data low-pass filter limits (e.g., 16, 32,  $64f$ ). Each model consistently and incorrectly assigns high energy in the high frequencies, regardless of whether the test data contained any high-frequency information. This is a concerning failure mode indicating FNOs do *not* generalize both in the presence of frequencies greater than, *and* the absence of frequencies less than, those which were present in their training data. We perform corresponding experiments for the Burgers dataset with resolution 1024 and low-pass limits  $\in \{64, 128, 256, 512\}f$  and Navier Stokes dataset with resolution 510 and low-pass limits  $\in \{8, 16, 32, 255\}f$ , and observe the same failure mode (see Appendix C: Figs. 13-14). **We conclude that varying the frequency information at test time is effectively out-of-distribution inference** as the model was not trained on data with such variation in frequency information, and, therefore, it fails to generalize.

### 3.2 Zero-shot Multi-Resolution Inference

We study whether FNOs are capable of spatial multi-resolution inference: simultaneously changing the sampling rate and frequency information. For each dataset in {Darcy, Burgers, Navier Stokes}, we train a model on data at resolutions (128, 64, 32, 16), (1024, 512, 256, 128,), (510, 255, 128, 64), respectively. In Fig. 1, we see that models trained at low resolutions do not generalize to high resolutions. Similarly, in Fig. 5, we again see a failure to generalize, and instead observe high-frequency artifacts in the model predictions in multi-resolution settings. Further, for time-varying PDEs, such as Navier Stokes, we observe that these high frequency aliasing artifacts compound across time steps

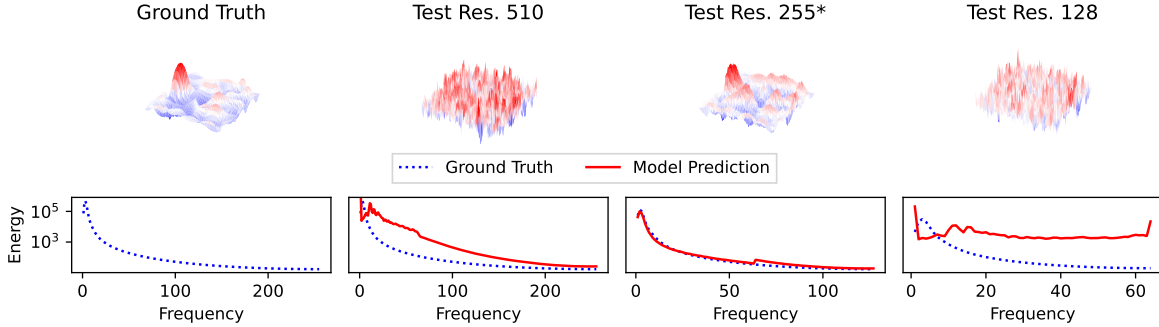


Figure 5: **FNOs do not generalize to higher or lower resolutions.** Model trained on Navier Stokes dataset at resolution 255 (indicated by \*), evaluated resolutions 510, 255, 128. **Top Row:** Ground truth, prediction at resolutions 510 (super-resolution), resolution 255 (same as train resolution), and resolution 128 (sub-resolution). **Bottom Row:** Average energy spectra over test data.

(see Appendix D: Fig. 15). In Appendix D: Fig. 16, we show that models trained at a given resolution do not achieve low loss across all test resolutions. In fact, losses vary by  $1\times$ ,  $2\times$ , and  $10\times$  across test resolutions for the Darcy, Burgers, and Navier Stokes datasets, respectively. **Therefore, we conclude that FNOs are not capable of consistent *zero-shot* super- or sub-resolution.**

## 4 Evaluating Potential Corrective Methods

In this section, we assess two previously proposed strategies for accurate zero-shot multi-resolution inference: physics-informed optimization objectives (Li et al., 2024b) and band-limited learning (Raonic et al., 2023; Gao et al., 2025). We find that neither enables accurate multi-resolution inference.

### 4.1 Physical Optimization Constraints

Physics-informed optimization constraints have been proposed as a means of achieving accurate inference in the *zero-shot* super-resolution setting (Li et al., 2024b). For each dataset in {Darcy, Burgers, Navier Stokes}, we train FNOs at all available resolutions. We optimize each set of model parameters  $\theta$  with a dual optimization objective  $\mathcal{L}(\theta) = (1 - w) * \ell_{\text{data}}(\theta) + w * \ell_{\text{phys}}(\theta)$ , where  $\ell_{\text{data}}$  is the original data-driven loss (mean squared error), and where  $\ell_{\text{phys}}$  is an additional physics-informed loss, which explicitly enforces that the governing PDE is satisfied. We use the physics losses of Li et al. (2024b), and we detail their implementation in Appendix E.

We find that the data-driven loss always outperforms any training objective that includes a physics constraint (see Appendix E: Fig. 17). We determine this by evaluating  $w \in \{0, 0.1, 0.25, 0.5\}$  for {Darcy, Burgers, Navier Stokes} at resolutions 64, 512, 255, respectively. Among the objectives that contain a physics constraint, we observe a clear trend: the lower the physics constraint is weighted, the better test performance the model achieves. This indicates that physics constraints make it more challenging for the model to be trained optimally despite extensive hyperparameter tuning (perhaps due to well known practical reasons such as being difficult to optimize (Krishnapriyan et al., 2021; Subramanian et al., 2022; Gao & Wang, 2023; Wang et al., 2023)).

To further illustrate this, we use the smallest non-zero  $w = 0.1$ , and compare the physics-informed optimization with solely data-driven optimization. In Fig. 6, the predicted spectra of data from models optimized with a physics loss generally diverge more substantially across test resolutions than models optimized with only a data loss. Models optimized with physics constraints even fail to accurately fit their training distributions (Fig. 6(c)), and they fail to generalize to both super- and sub-resolution data (Fig. 6(a,b,d)). See Appendix E for results on all datasets. We conclude that physics informed constraints do *not* reliably enable multi-resolution generalization.

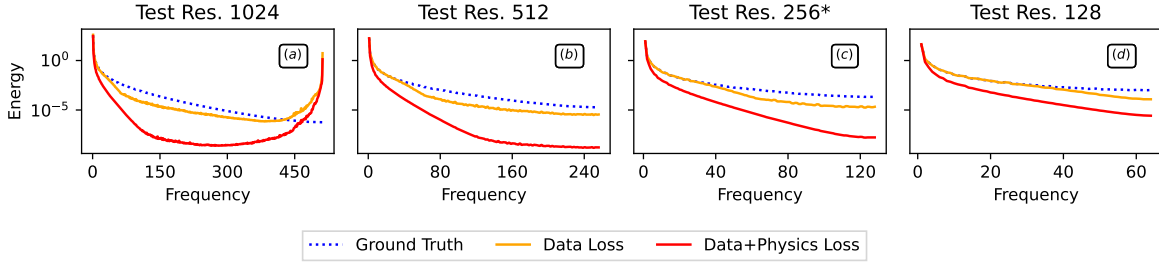


Figure 6: **(Physics-Informed) Optimization Evaluation.** FNO trained on Burgers data at resolution 256 (indicated by \*), with and without physics optimization constrains. Average test spectra are visualized. The spectra generated by the models trained with physics+data loss do not match the ground truth. (Physics Loss term weighting  $w = 10\%$ .) Full results are in [Appendix E](#), Figs. 19-21.

## 4.2 Band-limited Learning

We study two approaches which propose learning band-limited representations of data: convolutional neural operators (CNO) ([Raonic et al., 2023](#)); and the Cross-Resolution Operator-Learning (CROP) pipeline ([Gao et al., 2025](#)). Both CNO and CROP have been proposed as alias-free solutions to enable multi-resolution inference ([Bartolucci et al., 2023](#)). CNOs are *fixed-resolution* models; to use them, one must first interpolate their input to the model’s training resolution, do a forward pass, and then interpolate back to the original dimension. The CROP pipeline is more general and extends to any class of model by interpolating inputs (both at training and inference) to and from a fixed-dimensional representation before and after a forward pass.

We train and evaluate a CNO and CROP+FNO model on all {Darcy, Burgers, Navier Stokes} datasets. Models are optimized using optimal hyper-parameters which were found via a grid search detailed in [Appendix B](#). In [Fig. 7](#), we visualize the predicted spectra of models trained on resolution 16 data across test data of resolution {16, 32, 64, 128}. We observe that the CNO does accurately learn the band-limited representation of its training data. That is, the spectra matches that of the ground truth until frequency  $8f$ , after which, by design, it drops sharply. This means that while CNO does not alias, it cannot predict frequencies higher than what was seen during training. Similarly, we observe that the CROP model, accurately fits lower frequencies, but struggles to fit high frequencies accurately across resolutions.

We note more broadly that the design of band-limiting a model’s training data and predictive capacity is counter-intuitive to the goal of multi-resolution inference, in which, a broad range of frequencies must be modeled accurately. **Band-limiting a model’s predictive capacity may enable accurate fixed-resolution representations, but it ensures that high-frequency information is not predicted accurately (or at all).** We conclude that band-limited learning limits a model’s utility for *multi-resolution* inference (full results are in [Appendix F](#)).

## 5 Multi-Resolution Training

We hypothesize that the reason models struggle to do *zero-shot* multi-resolution inference is because data representing a physical system at varying resolutions is sufficiently *out-of-distribution* to the model’s fixed-resolution training data. To remedy this, we propose a data-driven solution: multi-resolution training (i.e., training on more than one resolution).

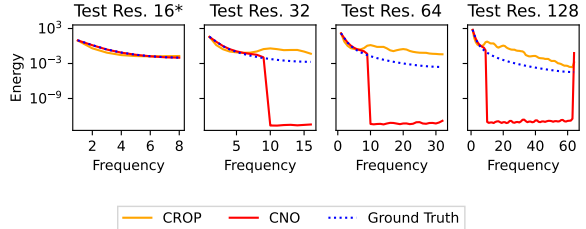


Figure 7: **Bandlimited Learning Evaluation.** Models trained on Darcy dataset at resolution 16 (indicated by \*), evaluated resolutions 16, 32, 64, 128. Average test set 2D energy spectrum of model predictions and ground truth. Notice both model prediction spectrums diverge from ground truth after frequency 8.

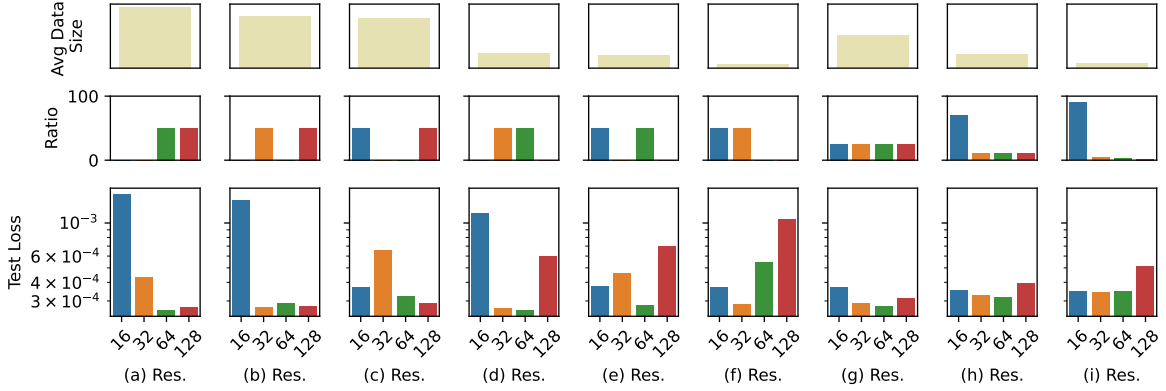


Figure 8: **Multi-resolution training.** FNO trained on multi-resolution Darcy data. **Top row:** Average number of pixels in a data sample in the training set. Lower number of pixels enables faster data generation and model training. **Middle row:** The ratios of data within each resolution bucket. **Bottom row:** The average test loss across different resolutions. Lower loss is better. Notice that mixed resolution datasets achieve both low average data size and low loss (ideal scenario).

We compose multi-resolution datasets by randomly sampling different proportions of training data at varying resolutions  $\{r_1, \dots, r_n\}$ , where  $r_x$  is the proportion of  $x$  resolution training data, and where  $n = 4$ . We begin by evaluating dual-resolution training. Li et al. (2024a) have previously shown that dual-resolution active learning enables more accurate *high-resolution* inference. We extend this finding and evaluate whether dual-resolution training can enable accurate *multi-resolution* inference. For each dataset in {Darcy, Burgers, Navier Stokes}, we combine data across resolutions in a pairwise manner creating  $\frac{n(n-1)}{2}$  dual-resolution sets; the ratio of data samples between the two resolutions is varied over  $p \in \{0.05, 0.1, 0.25, 0.5, 0.75, 0.9, 0.95\}$ . In Fig. 8(a-f), we observe for pair-wise training, the test performance for data that corresponds to the two training resolutions is generally better, but we also note that there are not consistent gains for the two non-training resolutions. This indicates that models perform best on the data resolutions on which they are trained.

To improve multi-resolution capabilities, we investigate the impact of including data from *all* resolutions. We first assess an equal number of samples across resolutions. In Fig. 8(g), the test performance across all resolutions improves, which confirms that multi-resolution training benefits multi-resolution inference. Next, we ask: *Can we improve the computationally efficiency of multi-resolution training?* To do this, the training dataset must be composed of primarily low resolution data, as it is both the cheapest to generate and the cheapest to train over (see Appendix G: Fig. 31). We compose two additional multi-resolution datasets:  $\{(0.7, 0.1, 0.1, 0.1), (0.9, 0.5, 0.3, 0.2)\}$ . In Fig. 8(h, i), models remain competitive across test resolutions, even as we decrease the amount of high-resolution data. In Fig. 9, we observe the consistent trend for all datasets: models are able to achieve a balance between dataset size and multi-resolution test loss via multi-resolution training. Optimizing the ratios across all resolutions remains an exciting future direction. Full results can be found in Appendix G.

## 6 Related Work

**Modeling PDEs via Deep Learning.** Three prominent approaches exist to discretely model PDEs with deep learning. **1) Mesh-Free** models learn the solution operator to a *specific* instance of a PDE (Yu et al., 2018; Raissi et al., 2019; Bar & Sochen, 2019; Smith et al., 2020; Pan & Duraisamy, 2020). Mesh-free models can be queried to return a measurement at any time and space coordinate. While this means that a single model can resolve its solution at arbitrary discretization, this approach has two shortcomings: (i) Inference costs increases with number of points queried; and (ii) Models cannot generalize beyond the specific PDE instance it was trained on. **2) Fixed-Mesh** models remedy both issues by learning a solution operator for a PDE *family* over a fixed-resolution mesh (Guo et al., 2016; Zhu & Zabaras, 2018; Adler & Öktem, 2017; Bhatnagar et al., 2019; Khoo et al., 2021). The inference costs of fixed-mesh models are lower than traditional numerical methods at corresponding

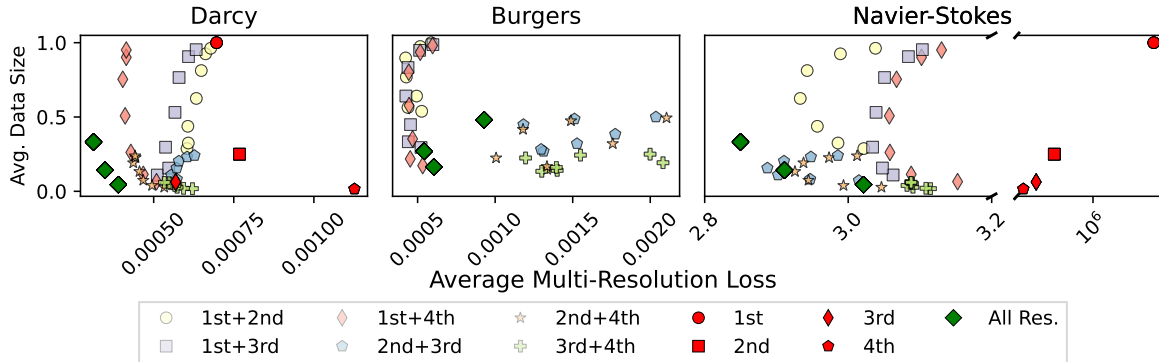


Figure 9: **Data Cost vs. Loss Tradeoff.** Lower data size and test loss are desirable (bottom left corner). We generally notice the “All Res.” datasets form the Pareto front of achieving optimal data size vs. test loss. “ $m$ ” and “ $m+n$ ” indicate the one or two resolutions that were included in the training set. “All Res.” indicates that dataset contains points from all resolutions available. “Avg. Data Size” is the normalized average number of pixels in a data point.

mesh resolutions. However, fixed-mesh models fall short when one is interested in modeling scale phenomena that cannot be resolved via the fixed-mesh resolution (e.g., high-frequency information in turbulent systems). **3) Mesh-invariant** models, unlike fixed-mesh models, are capable of doing inference at arbitrary mesh resolutions (Li et al., 2020b,a; Lu et al., 2021; Bhattacharya et al., 2021; Nelsen & Stuart, 2021; Patel et al., 2021; Rahman et al., 2022; Fanaskov & Oseledets, 2023). These methods have been proposed as a means to learn **mesh-invariant** solution operators to entire PDE families cheaply: train on low-resolution data, and use in a zero-shot fashion on arbitrary resolution data (e.g., zero-shot multi-resolution). In this work, we examine the zero-shot multi-resolution utility of mesh-invariant models.

**Aliasing (and corrective measures) in Deep Learning.** Sources of aliasing in deep learning include both artifacts of a pixel grid (which models learn and amplify) and the application of point-wise non-linearities to intermediate model representations (Karras et al., 2021; Gruver et al., 2022; Wilson, 2025). A straightforward approach, first introduced in generative adversarial networks, to stem nonlinearity-caused aliasing is to up sample a signal before applying a non-linearity, followed by down sampling the signal (Karras et al., 2021). Bartolucci et al. (2023) and Raonic et al. (2023) extend the application of an anti-alias activation function design to scientific machine learning. This does prevent *aliasing*, but it does not enable models trained at a specific resolution to resolve higher frequencies in higher resolution data. Gao et al. (2025) proposed a framework that “lifts” arbitrarily discretization data to a fixed-resolution band-limited space, both to train a model and to perform inference. We investigate the sources of aliasing the context of *zero-shot* multi-resolution inference, and we show that proposed solutions fall short in remedying the core issue: challenges with out-of-distribution generalization.

## 7 Conclusion and Future Work

For MLOs to be as versatile as numerical methods-based approaches for modeling PDEs, they must be able to perform accurate multi-resolution inference. To better understand an MLO’s abilities, we break down the task of multi-resolution inference by assessing a trained model’s ability both to *extrapolate* to higher/lower frequency information in data and to *interpolate* across varying data resolutions. We find that models trained on low resolution data and used for inference on high-resolution data can neither extrapolate nor interpolate; and, more generally, they fail to achieve accurate multi-resolution inference. Changing the resolution of data at inference time is akin to out-of-distribution inference: models have not learned how to generalize in such settings. We document that models used in a *zero-shot* multi-resolution setting are prone to aliasing. We study the utility of two existing solutions—physics-informed constrains and learning band-limited learning—and find that neither enable accurate multi-resolution inference.

Based on these results, we introduce a simple, intuitive, and principled approach to enable accurate multi-resolution inference: multi-resolution training. We show that models perform best at resolutions on which they have been trained; and we demonstrate that one can computationally efficiently achieve the benefits of multi-resolution training via datasets composed with mostly low-resolution data and small amounts of high-resolution data. This enables accurate multi-resolution learning, with the added benefit of low data-generation and model training cost. A promising future direction remains the automated selection of multi-resolution training data using strategies like active learning.

## Acknowledgements

This material is based upon work supported by the U.S. Department of Energy, Office of Science, Office of Advanced Scientific Computing Research, Department of Energy Computational Science Graduate Fellowship under Award Number DE-SC0023112.

## References

- Jonas Adler and Ozan Öktem. Solving ill-posed inverse problems using iterative deep neural networks. *Inverse Problems*, 33(12):124007, 2017.
- Reza Alizadeh, Janet K Allen, and Farrokh Mistree. Managing computational complexity using surrogate models: A critical review. *Research in Engineering Design*, 31(3):275–298, 2020.
- Michael J Asher, Barry FW Croke, Anthony J Jakeman, and Luk JM Peeters. A review of surrogate models and their application to groundwater modeling. *Water Resources Research*, 51(8):5957–5973, 2015.
- Kamyar Azizzadenesheli, Nikola Kovachki, Zongyi Li, Miguel Liu-Schiaffini, Jean Kossaifi, and Anima Anandkumar. Neural operators for accelerating scientific simulations and design. *Nature Reviews Physics*, 6(5):320–328, 2024.
- Leah Bar and Nir Sochen. Unsupervised deep learning algorithm for PDE-based forward and inverse problems. *arXiv preprint arXiv:1904.05417*, 2019.
- Francesca Bartolucci, Emmanuel de Bezenac, Bogdan Raonic, Roberto Molinaro, Siddhartha Mishra, and Rima Alaifari. Representation equivalent neural operators: A framework for alias-free operator learning. *Advances in Neural Information Processing Systems*, 36:69661–69672, 2023.
- Marsha J Berger and Joseph Oliger. Adaptive mesh refinement for hyperbolic partial differential equations. *Journal of computational Physics*, 53(3):484–512, 1984.
- Saakaar Bhatnagar, Yaser Afshar, Shaowu Pan, Karthik Duraisamy, and Shailendra Kaushik. Prediction of aerodynamic flow fields using convolutional neural networks. *Computational Mechanics*, 64(2):525–545, 2019.
- Kaushik Bhattacharya, Bamdad Hosseini, Nikola B Kovachki, and Andrew M Stuart. Model reduction and neural networks for parametric PDEs. *The SMAI journal of computational mathematics*, 7:121–157, 2021.
- Ashesh Chattopadhyay, Y. Qiang Sun, and Pedram Hassanzadeh. Challenges of learning multi-scale dynamics with AI weather models: Implications for stability and one solution, 2024. URL <https://arxiv.org/abs/2304.07029>.
- Alison Cozad, Nikolaos V Sahinidis, and David C Miller. Learning surrogate models for simulation-based optimization. *AIChE Journal*, 60(6):2211–2227, 2014.
- Vladimir Sergeevich Fanaskov and Ivan V Oseledets. Spectral neural operators. In *Doklady Mathematics*, volume 108, pp. S226–S232. Springer, 2023.
- Alexander Forrester, Andras Sobester, and Andy Keane. *Engineering design via surrogate modelling: A practical guide*. John Wiley & Sons, 2008.

- Wenhan Gao and Chunmei Wang. Active learning based sampling for high-dimensional nonlinear partial differential equations. *Journal of Computational Physics*, 475:111848, 2023.
- Wenhan Gao, Ruichen Xu, Yuefan Deng, and Yi Liu. Discretization-invariance? On the discretization mismatch errors in neural operators. In *The Thirteenth International Conference on Learning Representations*, 2025.
- Robert Joseph George, Jiawei Zhao, Jean Kossaifi, Zongyi Li, and Anima Anandkumar. Incremental spatial and spectral learning of neural operators for solving large-scale PDEs. *Transactions on Machine Learning Research*, 2024. URL <https://openreview.net/forum?id=xI6cPQ0bp0>.
- Nate Gruver, Marc Finzi, Micah Goldblum, and Andrew Gordon Wilson. The Lie derivative for measuring learned equivariance. *arXiv preprint arXiv:2210.02984*, 2022.
- Xiaoxiao Guo, Wei Li, and Francesco Iorio. Convolutional neural networks for steady flow approximation. In *Proceedings of the 22nd ACM SIGKDD international conference on knowledge discovery and data mining*, pp. 481–490, 2016.
- Tero Karras, Miika Aittala, Samuli Laine, Erik Härkönen, Janne Hellsten, Jaakko Lehtinen, and Timo Aila. Alias-free generative adversarial networks. *Advances in neural information processing systems*, 34:852–863, 2021.
- Yuehaw Khoo, Jianfeng Lu, and Lexing Ying. Solving parametric PDE problems with artificial neural networks. *European Journal of Applied Mathematics*, 32(3):421–435, 2021.
- Nikola Kovachki, Zongyi Li, Burigede Liu, Kamyar Azizzadenesheli, Kaushik Bhattacharya, Andrew Stuart, and Anima Anandkumar. Neural operator: Learning maps between function spaces with applications to PDEs. *Journal of Machine Learning Research*, 24(89):1–97, 2023.
- Aditi Krishnapriyan, Amir Gholami, Shandian Zhe, Robert Kirby, and Michael W Mahoney. Characterizing possible failure modes in physics-informed neural networks. *Advances in neural information processing systems*, 34:26548–26560, 2021.
- David Krueger, Ethan Caballero, Joern-Henrik Jacobsen, Amy Zhang, Jonathan Binas, Dinghui Zhang, Remi Le Priol, and Aaron Courville. Out-of-distribution generalization via risk extrapolation (rex). In *International conference on machine learning*, pp. 5815–5826. PMLR, 2021.
- Jakub Kudela and Radomil Matousek. Recent advances and applications of surrogate models for finite element method computations: A review. *Soft Computing*, 26(24):13709–13733, 2022.
- Shibo Li, Xin Yu, Wei Xing, Robert Kirby, Akil Narayan, and Shandian Zhe. Multi-resolution active learning of Fourier neural operators. In *Proceedings of The 27th International Conference on Artificial Intelligence and Statistics*, volume 238 of *Proceedings of Machine Learning Research*, pp. 2440–2448. PMLR, 02–04 May 2024a. URL <https://proceedings.mlr.press/v238/li24k.html>.
- Zongyi Li, Nikola Kovachki, Kamyar Azizzadenesheli, Burigede Liu, Kaushik Bhattacharya, Andrew Stuart, and Anima Anandkumar. Fourier neural operator for parametric partial differential equations. *arXiv preprint arXiv:2010.08895*, 2020a.
- Zongyi Li, Nikola Kovachki, Kamyar Azizzadenesheli, Burigede Liu, Kaushik Bhattacharya, Andrew Stuart, and Anima Anandkumar. Neural operator: Graph kernel network for partial differential equations. *arXiv preprint arXiv:2003.03485*, 2020b.
- Zongyi Li, Hongkai Zheng, Nikola Kovachki, David Jin, Haoxuan Chen, Burigede Liu, Kamyar Azizzadenesheli, and Anima Anandkumar. Physics-informed neural operator for learning partial differential equations. *ACM / IMS J. Data Sci.*, 1(3), May 2024b. URL <https://doi.org/10.1145/3648506>.
- Weitang Liu, Xiaoyun Wang, John Owens, and Yixuan Li. Energy-based out-of-distribution detection. *Advances in neural information processing systems*, 33:21464–21475, 2020.

- Lu Lu, Pengzhan Jin, Guofei Pang, Zhongqiang Zhang, and George Em Karniadakis. Learning non-linear operators via DeepONet based on the universal approximation theorem of operators. *Nature machine intelligence*, 3(3):218–229, 2021.
- Nicholas H Nelsen and Andrew M Stuart. The random feature model for input-output maps between banach spaces. *SIAM Journal on Scientific Computing*, 43(5):A3212–A3243, 2021.
- Katharina Ott, Prateek Katiyar, Philipp Hennig, and Michael Tiemann. ResNet after all: Neural ODEs and their numerical solution. In *International Conference on Learning Representations*, 2021.
- Shaowu Pan and Karthik Duraisamy. Physics-informed probabilistic learning of linear embeddings of nonlinear dynamics with guaranteed stability. *SIAM Journal on Applied Dynamical Systems*, 19(1):480–509, 2020.
- Ravi G Patel, Nathaniel A Trask, Mitchell A Wood, and Eric C Cyr. A physics-informed operator regression framework for extracting data-driven continuum models. *Computer Methods in Applied Mechanics and Engineering*, 373:113500, 2021.
- Alejandro F Queiruga, N Benjamin Erichson, Dane Taylor, and Michael W Mahoney. Continuous-in-depth neural networks. *arXiv preprint arXiv:2008.02389*, 2020.
- Md Ashiqur Rahman, Zachary E Ross, and Kamyar Azizzadenesheli. U-NO: U-shaped neural operators. *arXiv preprint arXiv:2204.11127*, 2022.
- Maziar Raissi, Paris Perdikaris, and George E Karniadakis. Physics-informed neural networks: A deep learning framework for solving forward and inverse problems involving nonlinear partial differential equations. *Journal of Computational physics*, 378:686–707, 2019.
- Bogdan Raonic, Roberto Molinaro, Tim De Ryck, Tobias Rohner, Francesca Bartolucci, Rima Alaifari, Siddhartha Mishra, and Emmanuel de Bézenac. Convolutional neural operators for robust and accurate learning of PDEs. *Advances in Neural Information Processing Systems*, 36:77187–77200, 2023.
- Pu Ren, N Benjamin Erichson, Shashank Subramanian, Omer San, Zarija Lukic, and Michael W Mahoney. Superbench: A super-resolution benchmark dataset for scientific machine learning. *arXiv preprint arXiv:2306.14070*, 2023.
- C.E. Shannon. Communication in the presence of noise. *Proceedings of the IRE*, 37(1):10–21, 1949.
- Jonathan D Smith, Kamyar Azizzadenesheli, and Zachary E Ross. Eikonet: Solving the eikonal equation with deep neural networks. *IEEE Transactions on Geoscience and Remote Sensing*, 59(12):10685–10696, 2020.
- A Subel, Y Guan, A Chattopadhyay, and P Hassanzadeh. Explaining the physics of transfer learning a data-driven subgrid-scale closure to a different turbulent flow. *arXiv preprint arXiv:2206.03198*, 724, 2022.
- Shashank Subramanian, Robert M Kirby, Michael W Mahoney, and Amir Gholami. Adaptive self-supervision algorithms for physics-informed neural networks. *arXiv preprint arXiv:2207.04084*, 2022.
- Bruno Sudret, Stefano Marelli, and Joe Wiart. Surrogate models for uncertainty quantification: An overview. In *2017 11th European conference on antennas and propagation (EUCAP)*, pp. 793–797. IEEE, 2017.
- Makoto Takamoto, Timothy Praditia, Raphael Leiteritz, Daniel MacKinlay, Francesco Alesiani, Dirk Pflüger, and Mathias Niepert. PDEBench: An extensive benchmark for scientific machine learning. *Advances in Neural Information Processing Systems*, 35:1596–1611, 2022.
- Alasdair Tran, Alexander Mathews, Lexing Xie, and Cheng Soon Ong. Factorized fourier neural operators. *arXiv preprint arXiv:2111.13802*, 2021.
- Michael Unser. Sampling-50 years after Shannon. *Proceedings of the IEEE*, 88(4):569–587, 2002.

- Sifan Wang, Shyam Sankaran, Hanwen Wang, and Paris Perdikaris. An expert’s guide to training physics-informed neural networks. *arXiv preprint arXiv:2308.08468*, 2023.
- John M Whittaker. The “Fourier” theory of the cardinal function. *Proceedings of the Edinburgh Mathematical Society*, 1(3):169–176, 1928.
- Andrew Gordon Wilson. Deep learning is not so mysterious or different. *arXiv preprint arXiv:2503.02113*, 2025.
- Liu Yang, Siting Liu, Tingwei Meng, and Stanley J Osher. In-context operator learning with data prompts for differential equation problems. *Proceedings of the National Academy of Sciences*, 120(39):e2310142120, 2023.
- Bing Yu et al. The deep Ritz method: a deep learning-based numerical algorithm for solving variational problems. *Communications in Mathematics and Statistics*, 6(1):1–12, 2018.
- Yinhao Zhu and Nicholas Zabaras. Bayesian deep convolutional encoder-decoder networks for surrogate modeling and uncertainty quantification. *Journal of Computational Physics*, 366:415–447, 2018.

## A Data

We study three standard scientific datasets: Darcy, Burgers, and turbulent incompressible Navier Stokes, as released in PDEBench (Takamoto et al., 2022). We summarize each dataset here; for full details, see Takamoto et al. (2022):

**Darcy.** We study the steady-state solution of 2D Darcy Flow over the unit square with viscosity term  $a(x)$  as an input of the system. We learn the mapping from  $a(x)$  to the steady-state solution described by:

$$\begin{aligned} -\nabla(a(x)\nabla u(x)) &= f(x), x \in (0, 1)^2 \\ u(x) &= 0, x \in \partial(0, 1)^2. \end{aligned}$$

The force term is a constant value  $f = 1$ .

**Burgers.** We study Burgers' equation which is used to model the non-linear behavior and diffusion process in fluid dynamics:

$$\partial_t u(t, x) + \partial_x(u^2(t, x)/2) = v/\pi \partial_{xx} u(t, x), x \in (0, 1), t \in (0, 2] \quad (3)$$

$$u(0, x) = u_0(x), x \in (0, 1). \quad (4)$$

The diffusion coefficient is a constant value  $f = 0.001$ .

**(Turbulent) Inhomogeneous, Incompressible Navier Stokes.** We study a popular variant of the Navier Stokes equation: the incompressible version. This equation is used to model dynamics far lower than the speed of propagation of waves in the medium:

$$\nabla \cdot v = 0, \rho(\partial_t v + v \cdot \nabla v) = -\nabla p + \eta \Delta v. \quad (5)$$

Takamoto et al. (2022) employ an augmented form of (5) which includes a vector field forcing term  $u$ :

$$\rho(\partial_t v + v \cdot \nabla v) = -\nabla p + \eta \Delta v + u.$$

The viscosity is a constant value  $v=0.01$ . We convert the incompressible Navier Stokes dataset to vorticity form to enable direct comparison with Li et al. (2020a).

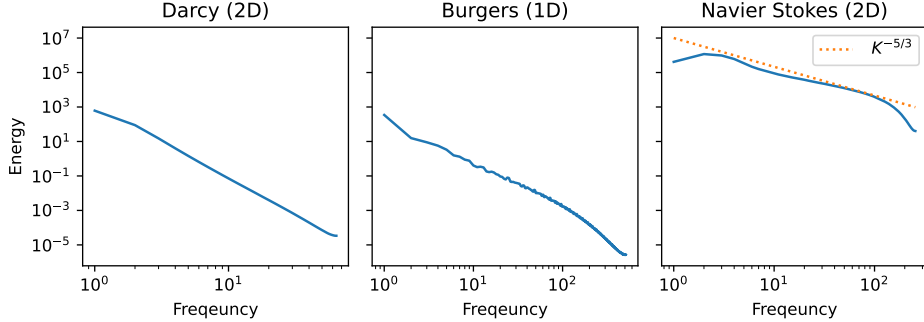


Figure 10: **Dataset Energy Spectrum.** Average energy spectra over test datasets. Notice that Navier Stokes is in the turbulent regime.  $K$  = Kolmogorov coefficient.

## B Hyper-parameter Search

**FNO Hyper-parameter Tuning.** For each dataset  $\in \{\text{Darcy, Burgers, Navier Stokes}\}$ , we do a grid search for optimal training hyper-parameters: learning rate  $\in \{1\text{e-}2, 1\text{e-}3, 1\text{e-}4, 1\text{e-}5\}$ ; and weight decay  $\in \{1\text{e-}5, 1\text{e-}6, 1\text{e-}7\}$ ; for both the data driven loss (i.e., mean squared error) and the respective data+physics driven loss. Each model was trained for 150 epochs. For the models optimized with the data+physics loss, we optimized the physics loss term’s weighting coefficient  $w \in \{0.1, 0.25, 0.5\}$ . For Darcy, Burgers, and Navier Stokes, we do this hyper-parameter search for data at resolution 64, 512, 255, respectively, and we then use the optimized parameter values for each dataset to train models at the remaining resolutions. See [Tab. 1](#) for the optimal hyper-parameter for each dataset/loss combination.

**CROP/CNO Hyper-parameter Tuning.** For each dataset  $\in \{\text{Darcy, Burgers, Navier Stokes}\}$ , we do a grid search for optimal training hyper-parameters: learning rate  $\in \{1\text{e-}3, 1\text{e-}4, 1\text{e-}5\}$ , for the data driven loss (i.e., mean squared error). Each model was trained for 150 epochs. For Darcy, Burgers, and Navier Stokes, we do this hyper-parameter search for data at resolution 64, 512, 255, respectively; and we then use the optimize parameter values for each dataset to train models at remaining resolutions. See [Tab. 2](#) for the optimal hyper-parameter for each dataset/loss combination.

Table 1: **Optimal FNO hyper-parameters** from hyper-parameter search outlined in Appendix B. \*NS batch size had to be reduced to 1 for multi-resolution training experiments (see [Sec. 5](#)), and therefore we used a lower learning rate in that setting.  $w$ =Physics Loss Coefficient (see [Sec. 4.1](#)).

Data	Loss	$w$	Learning Rate	Weight Decay	Batch Size
Darcy	Data	-	1e-3	1e-5	128
Darcy	Data+Physics	0.1	1e-2	1e-5	128
Burgers	Data	-	1e-3	1e-5	64
Burgers	Data+Physics	0.1	1e-3	1e-5	64
Navier Stokes	Data	-	1e-2	1e-6	4
Navier Stokes	Data+Physics	0.1	1e-4	1e-5	4
Navier Stokes*	Data	-	1e-5	1e-6	1

Table 2: **Optimal CNO/CROP hyper-parameters** from hyper-parameter search outlined in Appendix B. \*The original CROP implementation did not include a 1D version, so we omit CROP for the 1D Burgers dataset.

Data	Loss	Model	Learning Rate	Weight Decay	Batch Size
Darcy	Data	CNO	0.0001	1e-5	128
Darcy	Data	CROP	0.001	1e-5	128
Burgers*	Data	CNO	0.001	1e-5	64
Navier Stokes	Data	CNO	0.001	1e-6	1
Navier Stokes	Data	CROP	0.001	1e-6	1

## C Information Extrapolation and Resolution Interpolation

Here, we include the full experimental results of studying FNOs' abilities to do both information extrapolation and resolution interpolations, as described in [Sec. 3](#).

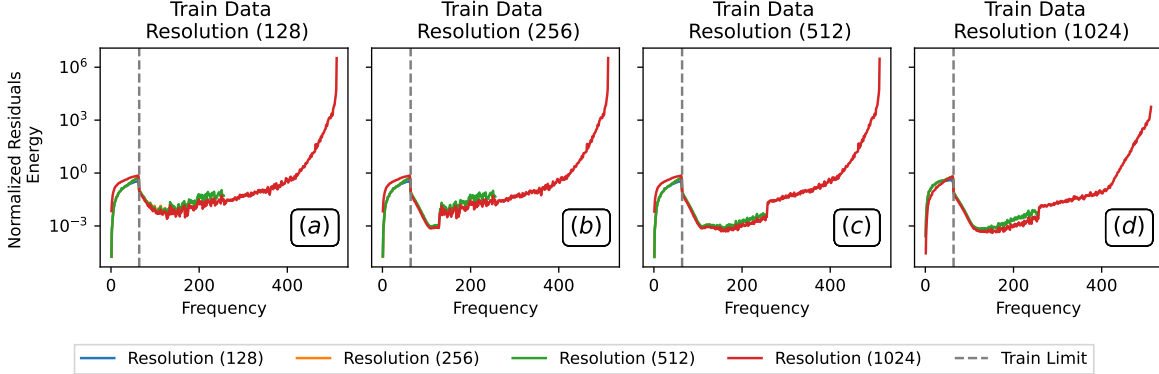


Figure 11: **Interpolation.** Four FNOs trained on Burgers data low-pass limit  $64f$  (constant frequency information) and down sampled to resolutions  $\{128, 256, 512, 1024\}$  (varying sampling rate) from left to right. We test if each model can generalize to data with varying sampling rate. We visualize the normalize residual spectra across test data. Notice that the residual spectra (error) increases substantially in the low frequencies. Lower energy at all wave numbers is better.

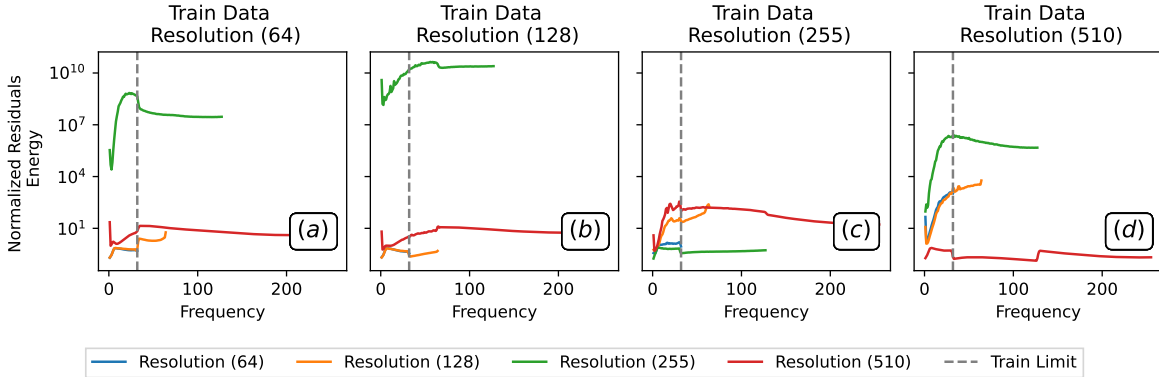


Figure 12: **Interpolation.** Four FNOs trained on Navier Stokes data low-pass limit  $32f$  (constant frequency information) and down sampled to resolutions  $\{64, 128, 255, 510\}$  (varying sampling rate) from left to right. We test if each model can generalize to data with varying sampling rate. We visualize the normalize residual spectra across test data. Notice that the residual spectra (error) increases substantially in the low frequencies. Lower energy at all wave numbers is better.

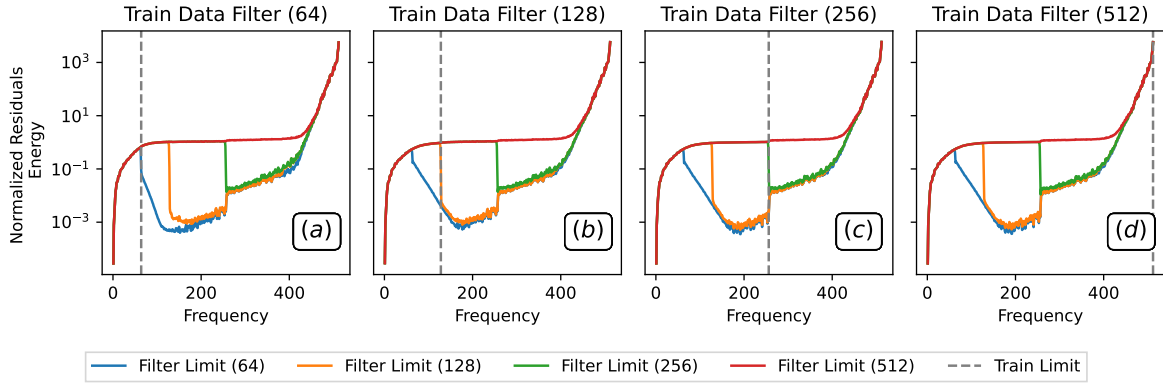


Figure 13: **Extrapolation.** Four FNOs trained on Burgers data of resolution 1024 (constant sampling rate) and low-pass filtered with limits  $\{64,128,256,512\}f$  (varying frequency information) from left to right. We test if each model can generalize to data with varying frequency information. We visualize the normalize residual spectra across test data. Notice that the residual spectra (error) increases substantially in the high frequencies. Lower residual energy at all wave numbers is better.

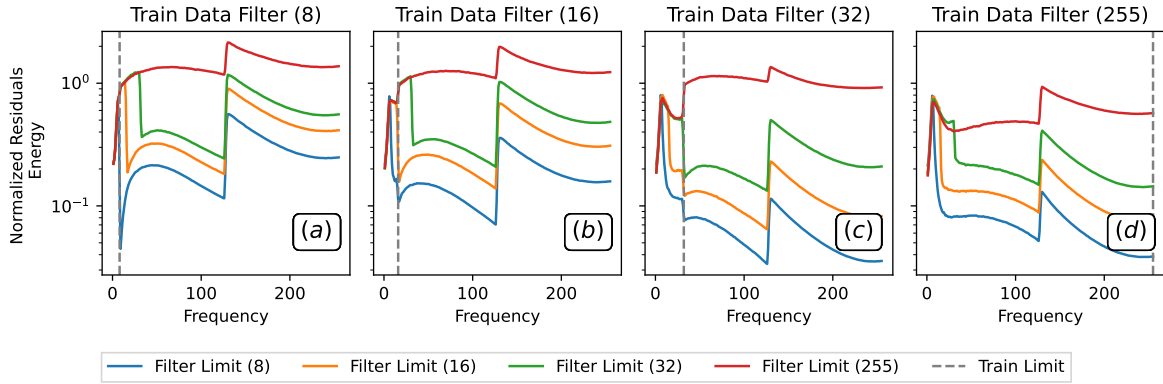


Figure 14: **Extrapolation.** Four FNOs trained on Navier Stokes data of resolution 510 (constant sampling rate) and low-pass filtered with limits  $\{8,16,32,255\}f$  (varying frequency information) from left to right. Test if each model can generalize to data with varying frequency information. We visualize the normalize residual spectra across test data. Notice that the residual spectra (error) increases substantially in the high frequencies. Lower residual energy at all wave numbers is better.

# D Evaluating Sub- and Super-Resolution

Here we included the full experiment results of studying FNOs’ abilities to do zero-shot multi-resolution inference as described in [Sec. 3](#).

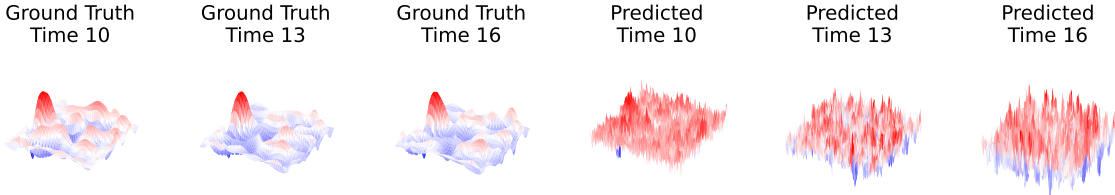


Figure 15: **Aliasing artifacts compound over time.** FNO trained on resolution 255 Navier-Stokes data, evaluated at resolution 510. **Left:** Ground truth evolution of NS fluid flow. **Right:** Corresponding FNO predictions at resolution 510. Notice that the high frequency artifacts become more prevalent over time.

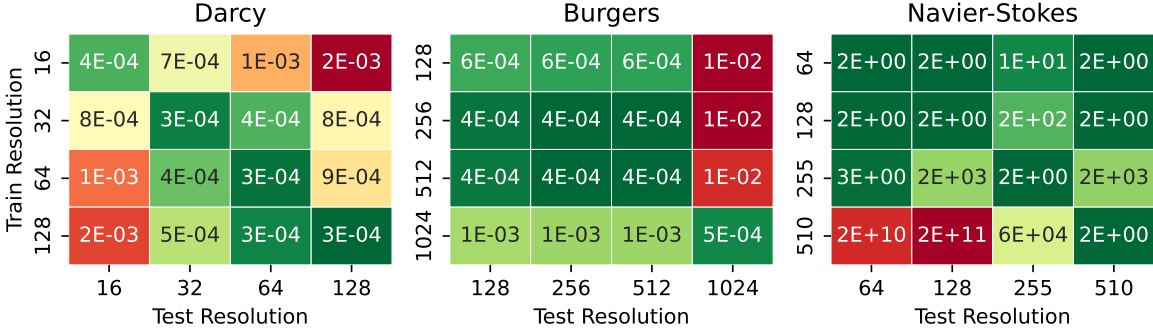


Figure 16: **FNOs do not reliably generalize to higher or lower resolutions.** Heatmaps of losses incurred by FNO trained and tested at varying resolutions (lower is better). When the test resolution varies from the training resolution, the models often incur a substantial increase in loss.

# E Physics-Informed Optimization

Here, we use the physics losses of Li et al. (2024b) which explicitly enforce that the governing PDE is satisfied. The governing PDEs are detailed in Appendix A.

Below we include the results of tuning the physics loss weighting coefficient  $w$  in Figs. 18 and 17. We then include the full comparisons of training each dataset (Darcy, Burgers, Navier Stokes) at each resolution with both  $w \in \{0, 0.1\}$  in Figs. 19-20.

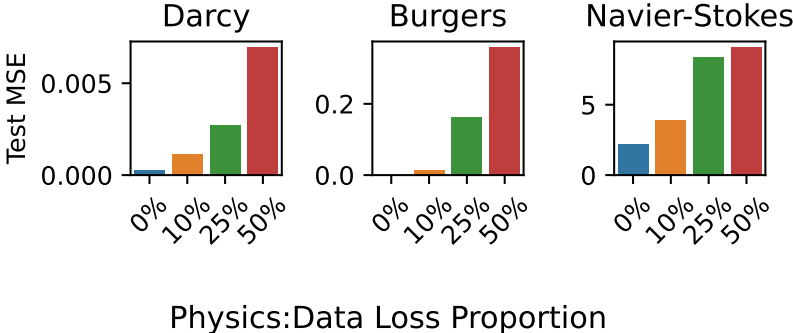


Figure 17: **(Physics-Informed) Optimization**. Increasing the proportion of physics-informed loss in the optimization objective corresponds to increased test loss. Lower MSE is better. Darcy trained at resolution 64, Burgers trained at resolution 512, and Navier Stokes trained at resolution 255.

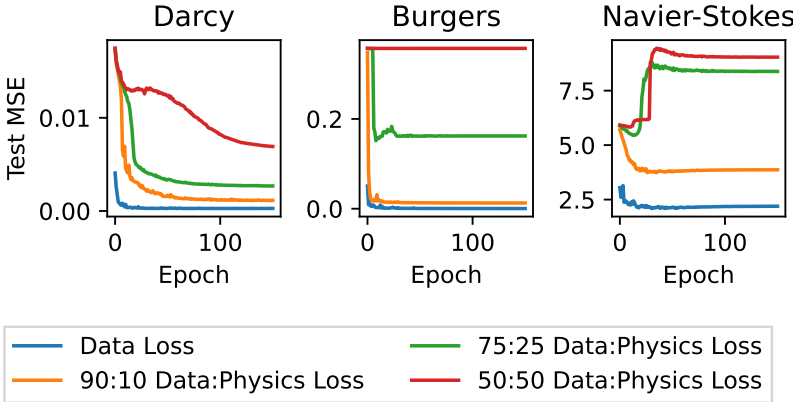


Figure 18: **(Physics-Informed) Optimization Objective**. Physics informed constraints never achieves better performance than using pure data-driven constraints. Darcy trained at resolution 64, Burgers trained at resolution 512, and Navier Stokes trained at resolution 255.

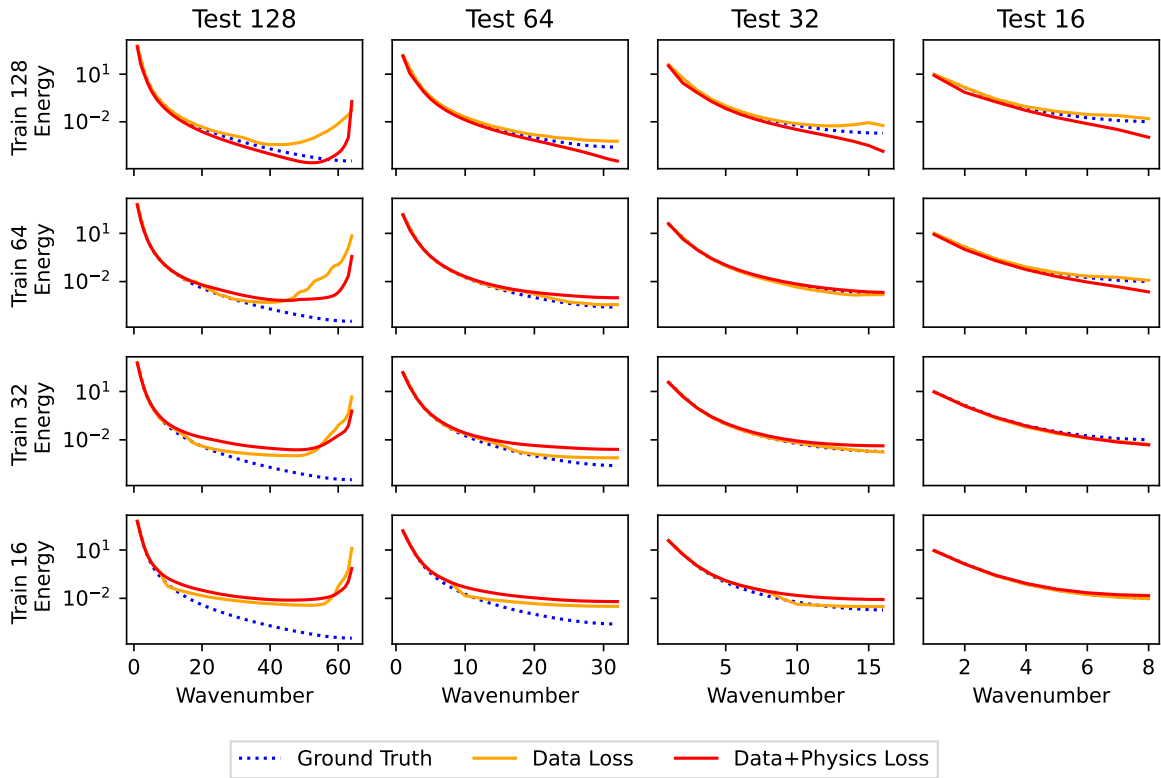


Figure 19: **Darcy**. Energy spectra for models trained at a specific resolution (y-axis) and tested at multiple resolution (x-axis), with and without physics optimization constraint. The spectra generated by the models trained with physics+data loss do not match ground truth. We set  $w = 10\%$ .

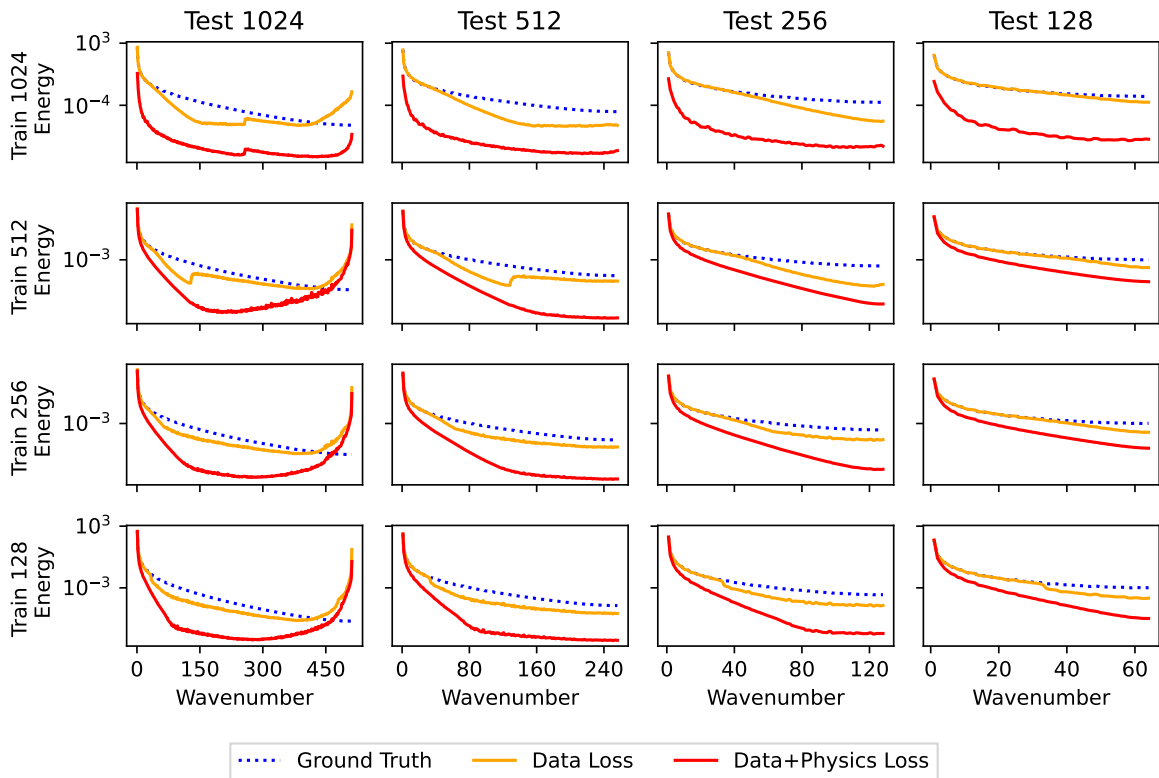


Figure 20: **Burgers**. Energy spectra for models trained at a specific resolution (y-axis) and tested at multiple resolution (x-axis), with and without physics optimization constraint. The spectra generated by the models trained with physics+data loss do not match ground truth. We set  $w = 10\%$ .

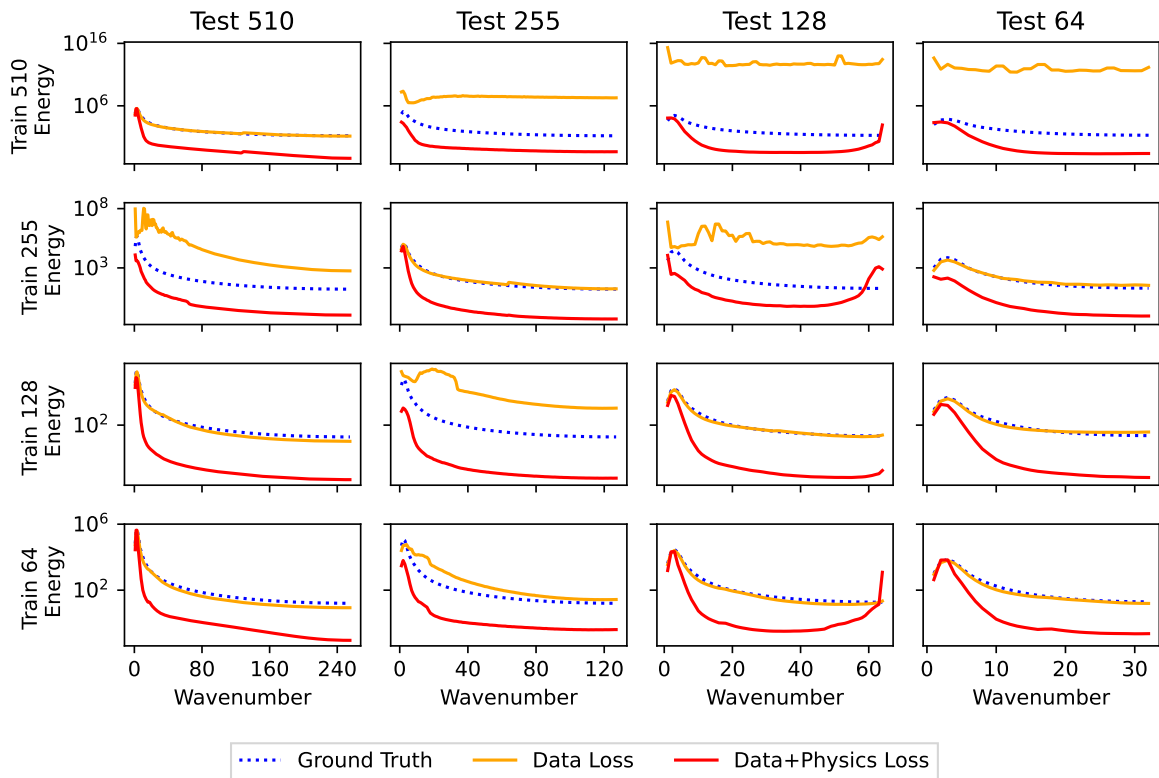


Figure 21: **Navier Stokes**. Energy spectra for models trained at a specific resolution (y-axis) and tested at multiple resolution (x-axis), with and without physics optimization constraint. The spectra generated by the models trained with physics+data loss do not match ground truth. We set  $w = 10\%$ .

## F Band-limited Learning

Here, we include the full experimental results of training models with mixed resolution datasets, as described in [Sec. 4.2](#). Note that [Gao et al. \(2025\)](#) did not release a 1D CROP pipeline; therefore, we were unable to test CROP with Burgers.

First, we observe that band-limited learning, in which models are able to both infer and learn over band-limited representations of data, accurately learns the frequency region of the data included in the band-limit. However, these models struggle to learn / do not learn anything outside this range (see [Figs. 7, 26, 24](#)). The implication of this is that band-limited-approaches suffice for modeling data within a prespecified range, as long as the band-limit range is wide enough, and the model will never need to be used to infer on data containing additional frequency information. However, we observe the band limited approach **under performs** multi-resolution training at fitting the full spectrum in the multi-resolution inference setting; this is because the resolution of data, and consequently the resolved frequencies, are changing ([Fig. 9](#)). For both Darcy ([Fig. 24](#)) and Burgers ([Fig. 25](#)), we notice that multi-resolution training out-performs band-limited approaches. In [Fig. 7](#), we observe that the predetermined band-limit leads to error in the high frequency range.

A scenario in which CNO and CROP *appear* to perform well is on datasets in which the majority of the energy is concentrated in the predetermined band-limit (e.g., Navier Stokes, see [Fig. 10](#)). In this setting, we see that band-limited fit the lower frequencies in the spectrum very well ([Fig. 26](#)). However, we also see in [Fig. 26](#), that multi-resolution training is the only method that consistently predicts both the correct amount of energy across the full spectrum. Band limited approaches *fail* to fit the high frequency range of the spectrum.

We note that band-limited approaches do not accurately fit frequencies outside of their predetermined limit. This makes them effective for fixed-resolution inference, but they are *ineffective* for multi-resolution inference. Alternatively, we demonstrated in [Sec. 5](#) that multi-resolution inference can be scaled to new data resolutions (and therefore new parts of the spectral energy spectrum) via scaling up representative samples in the training dataset. We conclude that multi-resolution training is a more flexible and scalable approach to enabling accurate multi-resolution training at *all* parts of the energy spectrum.

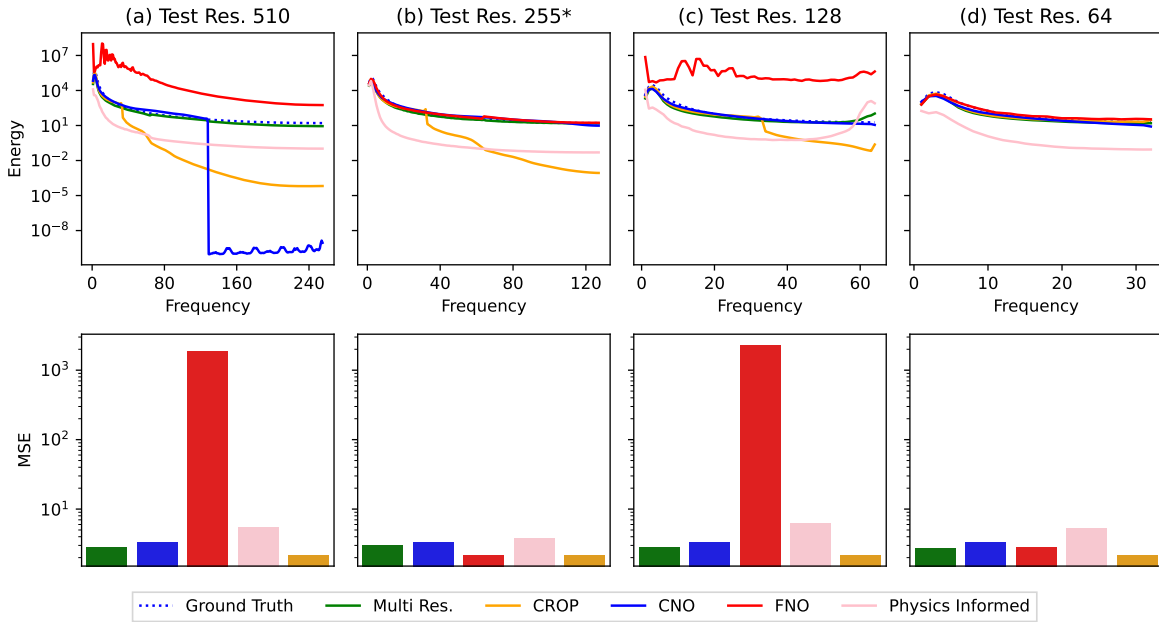


Figure 22: **Spectral Comparison Navier Stokes. Top Row:** Average predicted spectra for test data at varying resolutions across all methods. **Bottom row:** Average mean squared error loss over test data at varying resolutions across all methods. **Zero-shot methods:** CNO, FNO, Physics Informed and CROP are all zero-shot methods, meaning there are trained at a specific resolution (255, indicated by \*), and evaluated at resolutions 510, 255, 128, 64. **Data-driven method:** Multi-resolution training; notice that multi-resolution training is the only method that consistently fits both the high and low parts of the spectra. **Band-limited methods:** CNO and CROP are both band-limited methods which are trained in a zero-shot manner at a fixed resolution; we observe that they only accurately fit the low frequencies.

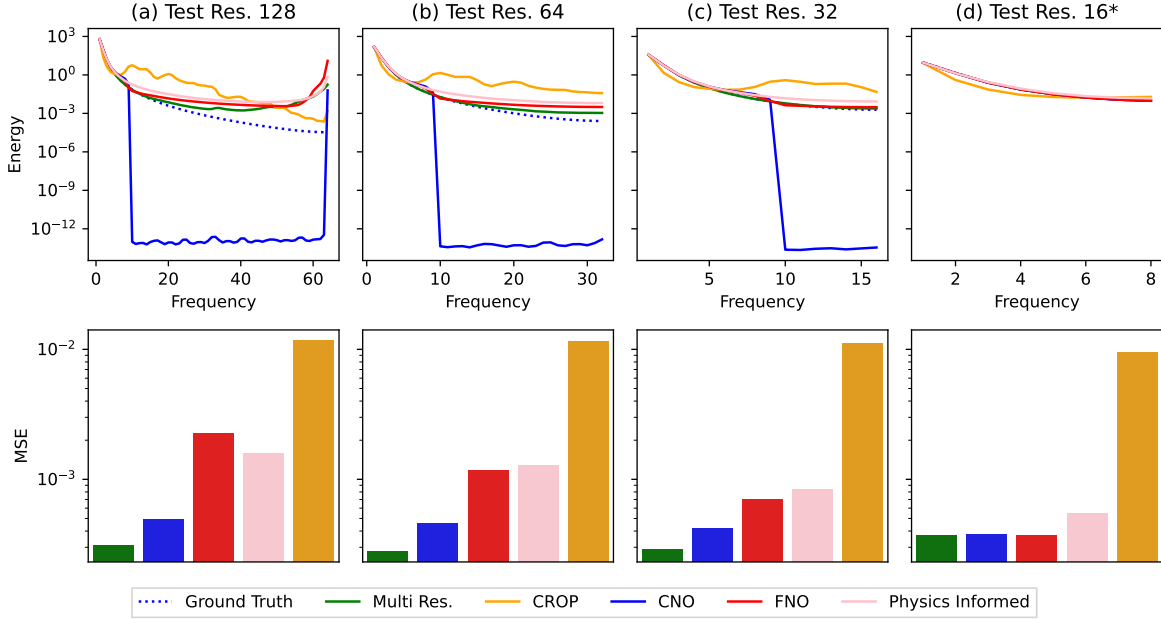


Figure 23: **Spectral Comparison Darcy. Top Row:** Average predicted spectra for test data at varying resolutions across all methods. **Bottom row:** Average mean squared error loss over test data at varying resolutions across all methods. **Zero-shot methods:** CNO, FNO, Physics Informed and CROP are all zero-shot methods, meaning there are trained at a specific resolution (16, indicated by \*), and evaluated at resolutions 128, 64, 32, 16. **Data-driven method:** Multi-resolution training; notice that multi-resolution training is the only method that consistently fits both the high and low parts of the spectra. **Band-limited methods:** CNO and CROP are both band-limited methods which are trained in a zero-shot manner at a fixed resolution; we observe that they only accurately fit the low frequencies.

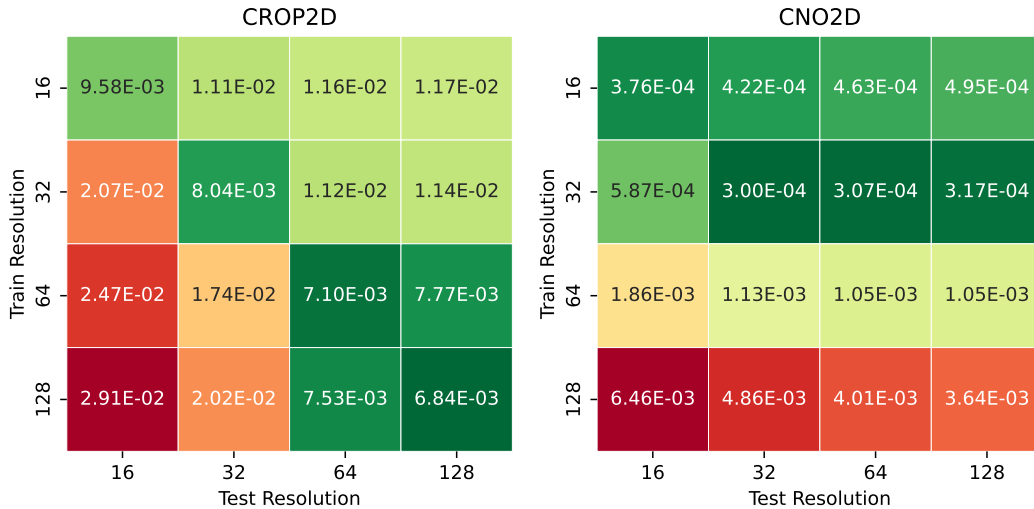


Figure 24: **CROP+FNO and CNO trained on Darcy.** On average, both CROP+FNO and CNO incur higher losses across resolutions compared to both FNO (Fig. 16) and multi-resolution training (Fig. 9).

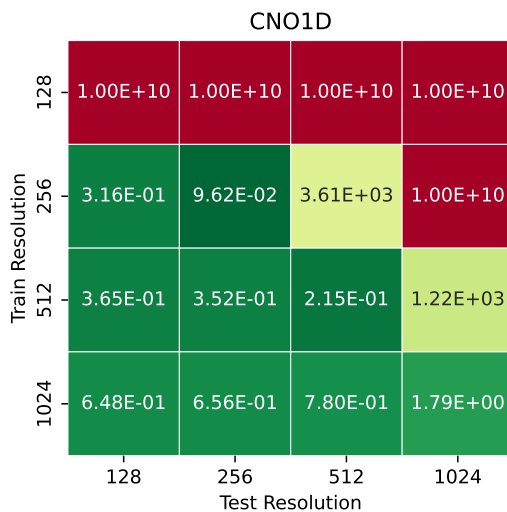


Figure 25: **CNO trained on Burgers.** On average, CNO incur higher losses across resolutions compared to both FNO (Fig. 16) and multi-resolution training (Fig. 9). We note that despite our hyperparameter search (Tab. 2) the CNO model trained on resolution 128 failed to converge.

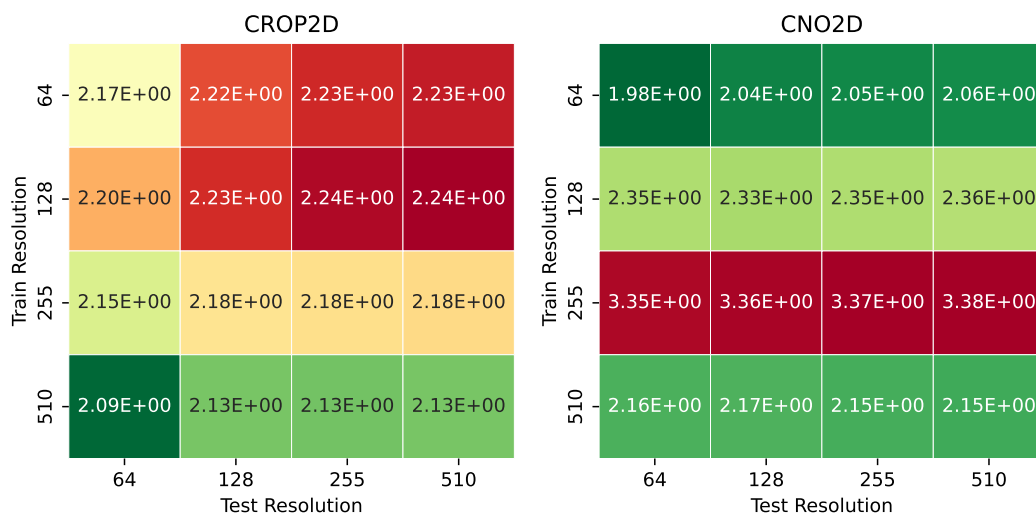


Figure 26: **CROP+FNO and CNO trained on Navier Stokes.** On average, both CROP+FNO and CNO incur lower losses across resolutions compared to both FNO (Fig. 16) and multi-resolution training (Fig. 9).

## G Multi-Resolution Training

Here, we include the full experimental results of training models with mixed resolution datasets, as described in Sec. 5. We provide an overview comparison across methods in Fig. 27. See Figs. 28-30 for our main results. We plot the association between increased dataset size and increased training time in Fig. 31.

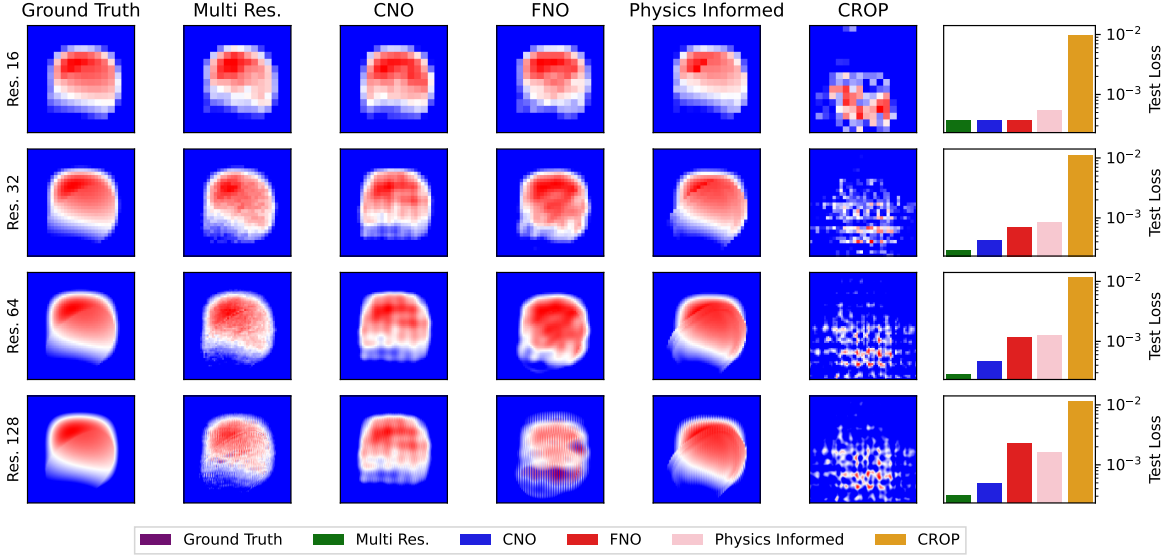


Figure 27: **Assessing multi-resolution inference.** Column 1: Expected prediction for Darcy flow at varying resolutions. Columns 2-6: Sample prediction for Darcy flow at varying test resolutions. Column 7: Average mean squared error test loss at each resolution (lower is better). **Zero-shot methods:** CNO, FNO, Physics Informed and CROP are all zero-shot methods, meaning the model was trained at a specific resolution (16) and evaluated at resolutions 16, 32, 64, 128. **Data-driven method:** Multi-resolution training; notice that multi-resolution training consistently outperforms zero-shot methods.

## H Model Implementations

The **Fourier Neural Operator** is described in detail in (Li et al., 2020a); we closely follow their implementation which can be found at <https://neuraloperator.github.io/dev/index.html>.

The **CNO** is described in detail in (Raonic et al., 2023); we closely follow their implementation which can be found at <https://github.com/camlab-ethz/ConvolutionalNeuralOperator/tree/main>.

The **CROP** pipeline is described in detail in (Gao et al., 2025); we closely follow their implementation for CROP+FNO which can be found at <https://github.com/wenhangao21/ICLR25-CROP/tree/main>. We note that they did not include a 1D CROP implementation, so we exclude evaluation of CROP on the 1D Burgers dataset.

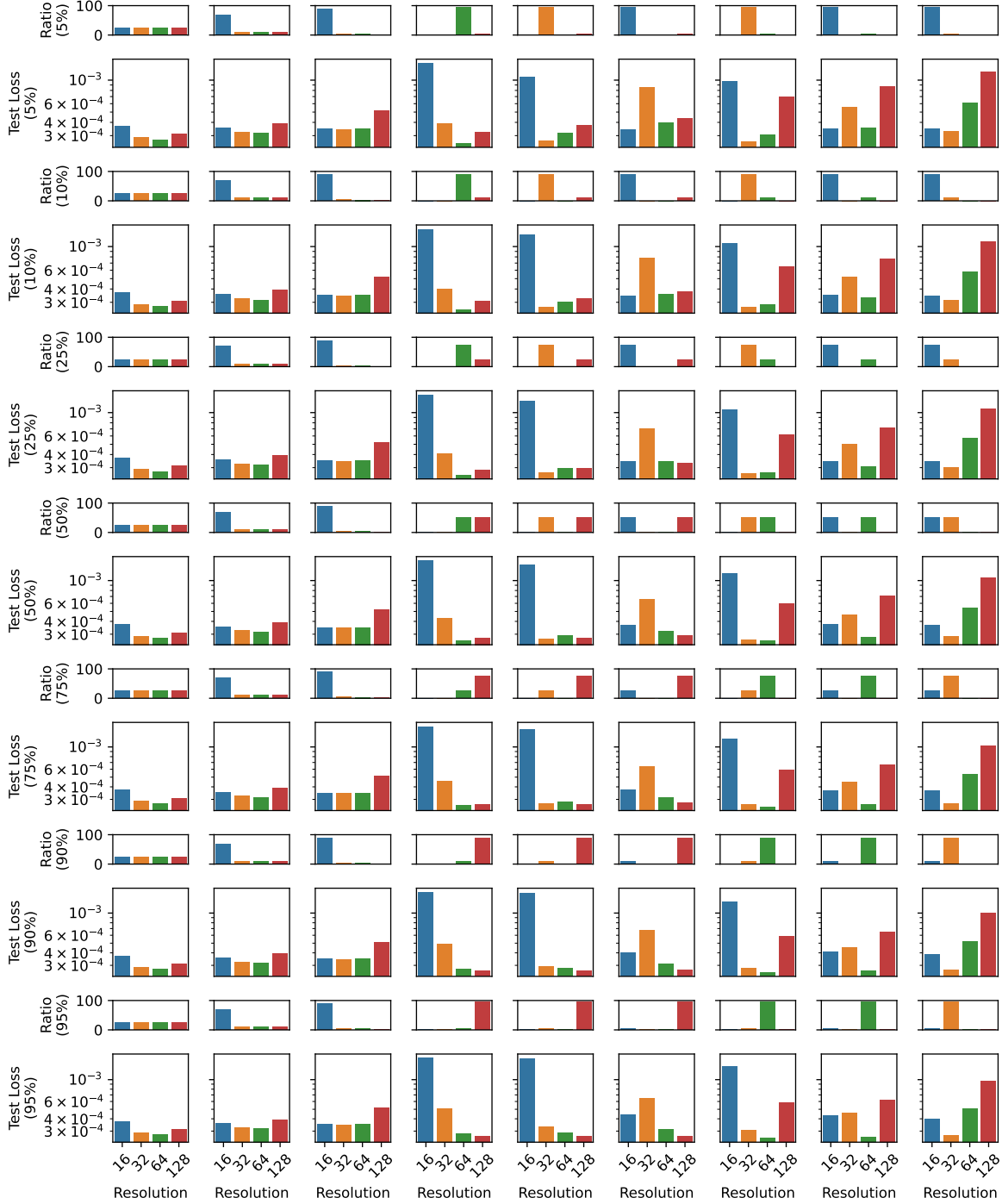


Figure 28: **Darcy Multi-Resolution Training.** FNO trained on multi-resolution Darcy data. Each row include two sub-rows; each row is delineated the the dual-resolution training ratio (indicated in y-axis label). The top sub-row illustrates the ratios of data within each resolution bucket. The bottom sub-row indicates the average test loss across different resolutions. Lower loss is better. Notice in the mixed resolution datasets achieve both low average data size and low loss (ideal scenario).

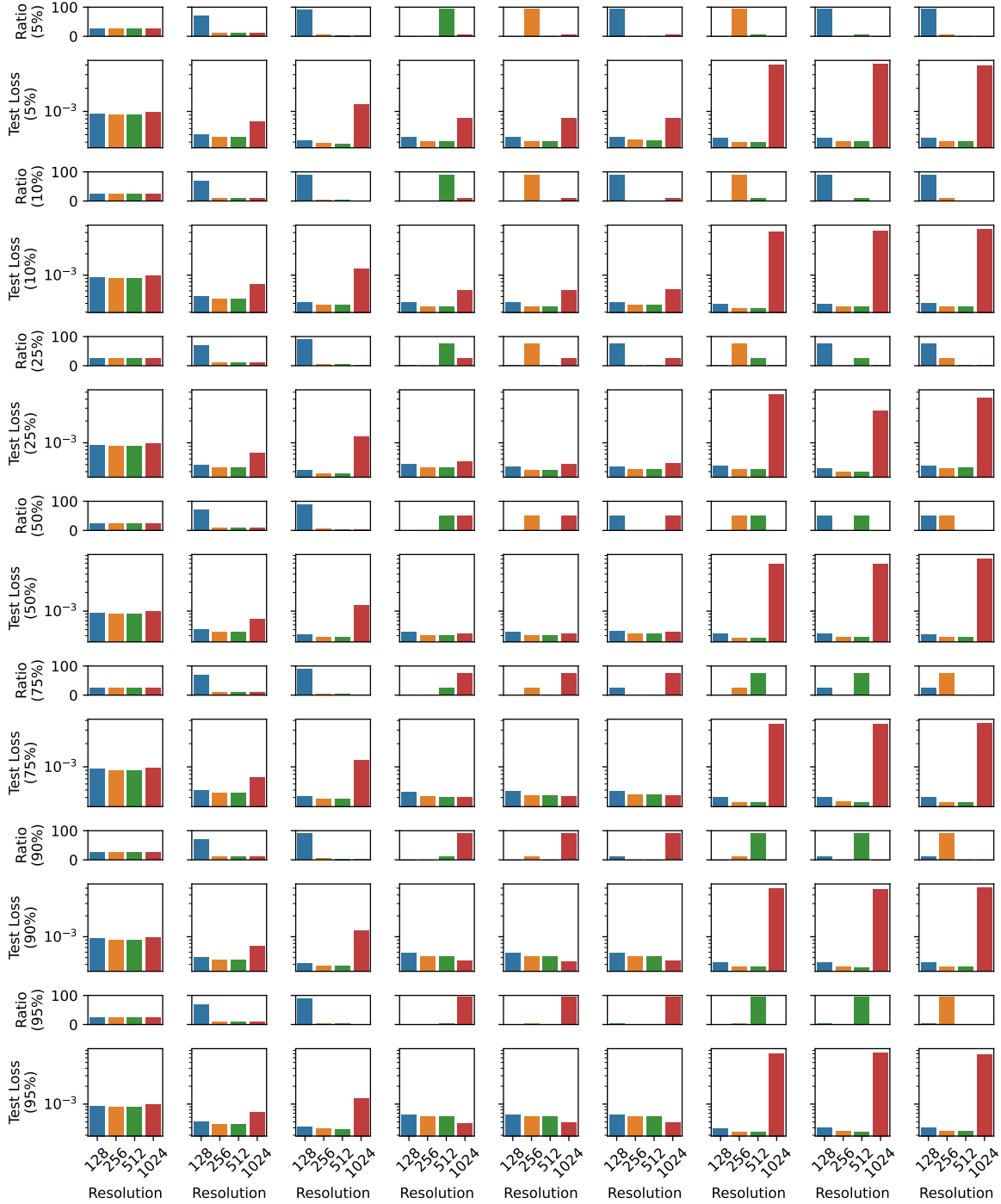


Figure 29: **Burgers Multi-Resolution Training.** FNO trained on multi-resolution Burgers data. Each row include two sub-rows; each row is delineated the the dual-resolution training ratio (indicated in y-axis label). The top sub-row illustrates the ratios of data within each resolution bucket. The bottom sub-row indicates the average test loss across different resolutions. Lower loss is better. Notice in the mixed resolution datasets achieve both low average data size and low loss (ideal scenario).

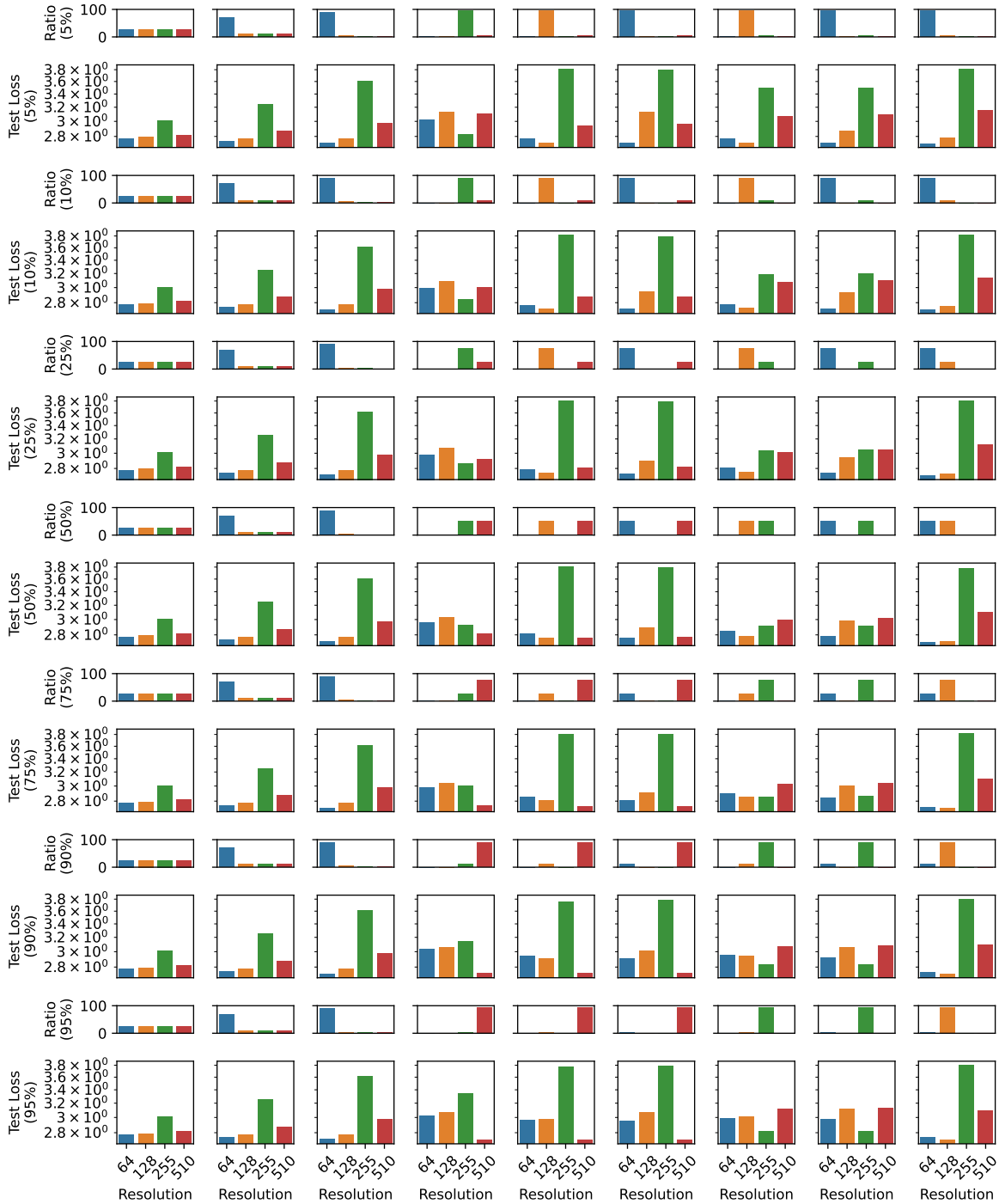


Figure 30: **Navier Stokes Multi-Resolution Training.** FNO trained on multi-resolution Navier Stokes data. Each row include two sub-rows; each row is delineated the the dual-resolution training ratio (indicated in y-axis label). The top sub-row illustrates the ratios of data within each resolution bucket. The bottom sub-row indicates the average test loss across different resolutions. Lower loss is better. Notice in the mixed resolution datasets achieve both low average data size and low loss (ideal scenario).

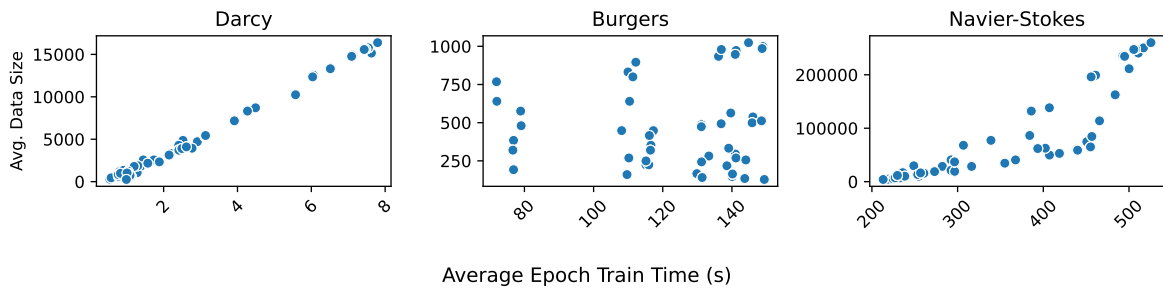


Figure 31: **Data size corresponds with training time.** We notice a clear trend with Darcy and Navier Stokes datasets: as data size increases, so does average training time per epoch. For Burgers, this trend is less clear. However, we note that the Burgers dataset is several orders of magnitude smaller and therefore can be used with a high batch size (see [Tab. 1](#)), which reduces the computational gains achieved from a smaller sized dataset.

# I Max Modes

A key design decision in the FNO architecture is the parameter  $m$  that indicates maximum frequencies to keep along each dimension in the Fourier layer during the forward pass. This has implications both during training (which frequencies are learned in the Fourier layers) and at inference (which frequencies are predicted over in the Fourier layers). In Sec. 3, the FNO is always initialized such that it can make use all frequencies in its input; this is especially critical in the multi-resolution setting where data of varying discretization will have varying frequency information. Here, we study the impact of varying  $m$ . In the zero-shot multi-resolution inference setting, in Figs. 33 and 32, we find that that across all variation in  $m$ , the models assign high energy in the high-frequencies (e.g., aliasing). More broadly, we comment that in the context of multi-resolution inference, it does not make sense to set  $m$  to a value less than the largest populated frequency in a model input, as it ensures that the model cannot make use that frequency information greater than  $m$  in the Fourier layers. In the event frequency information above  $m$  is not useful to prediction (e.g., noise), we advocate low-pass filtering and down sampling the data to a more compressed representation of data prior to inference to remove unwanted frequencies and ensure faster inference.

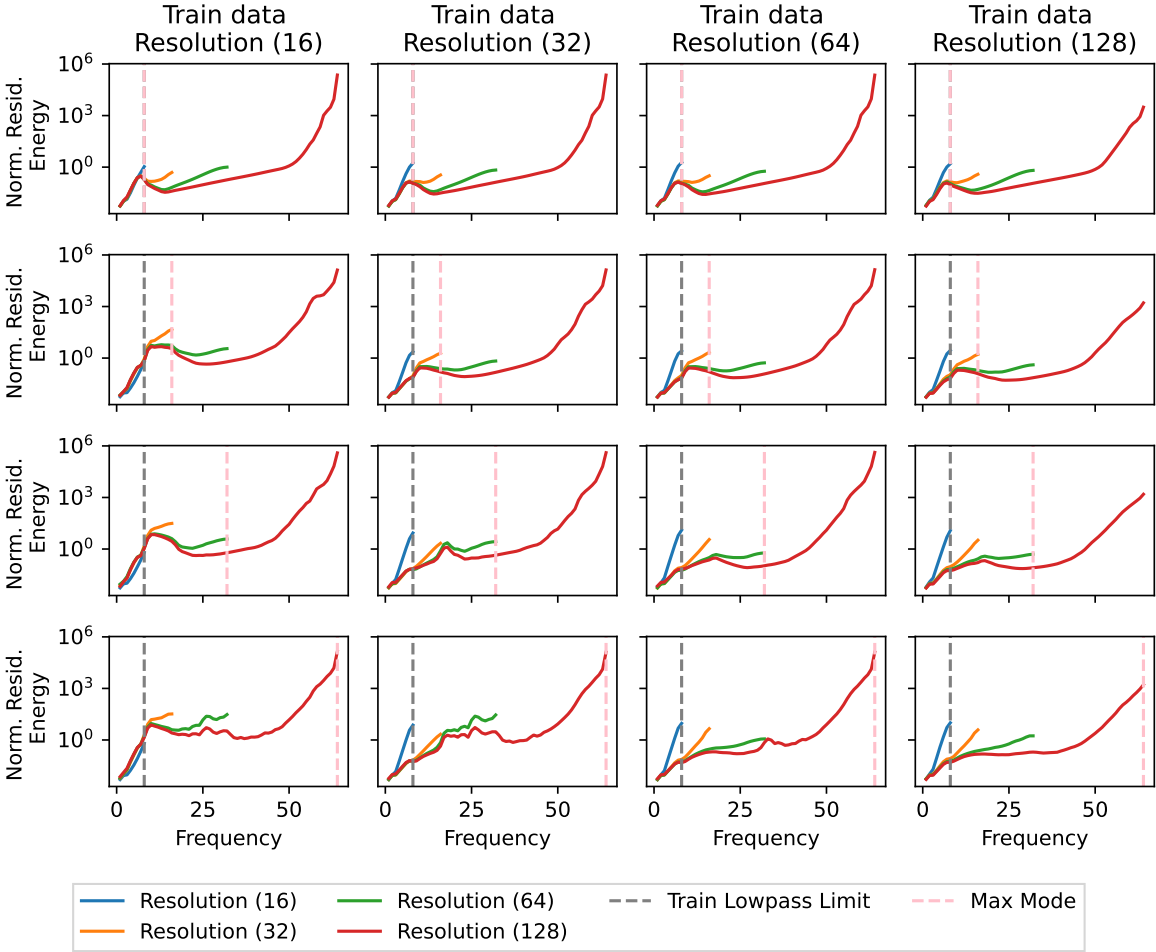


Figure 32: **Resolution Interpolation.** Four FNOs trained on Darcy data low-pass limit = 8 (constant frequency information) and down sampled to resolutions  $\{16,32,64,128\}$  (varying sampling rate) from left to right, and top to bottom with max modes  $m \in \{8,16,32,64\}$ . We test if each model can generalize to data with varying sampling rate. Visualizing the spectrum of the normalized residuals across test data. Notice that the residual spectra (error) increases substantially in the low frequencies. Lower energy at all wave numbers is better. We see that across all variation in  $m$ , the models assign high energy in the high-frequencies.

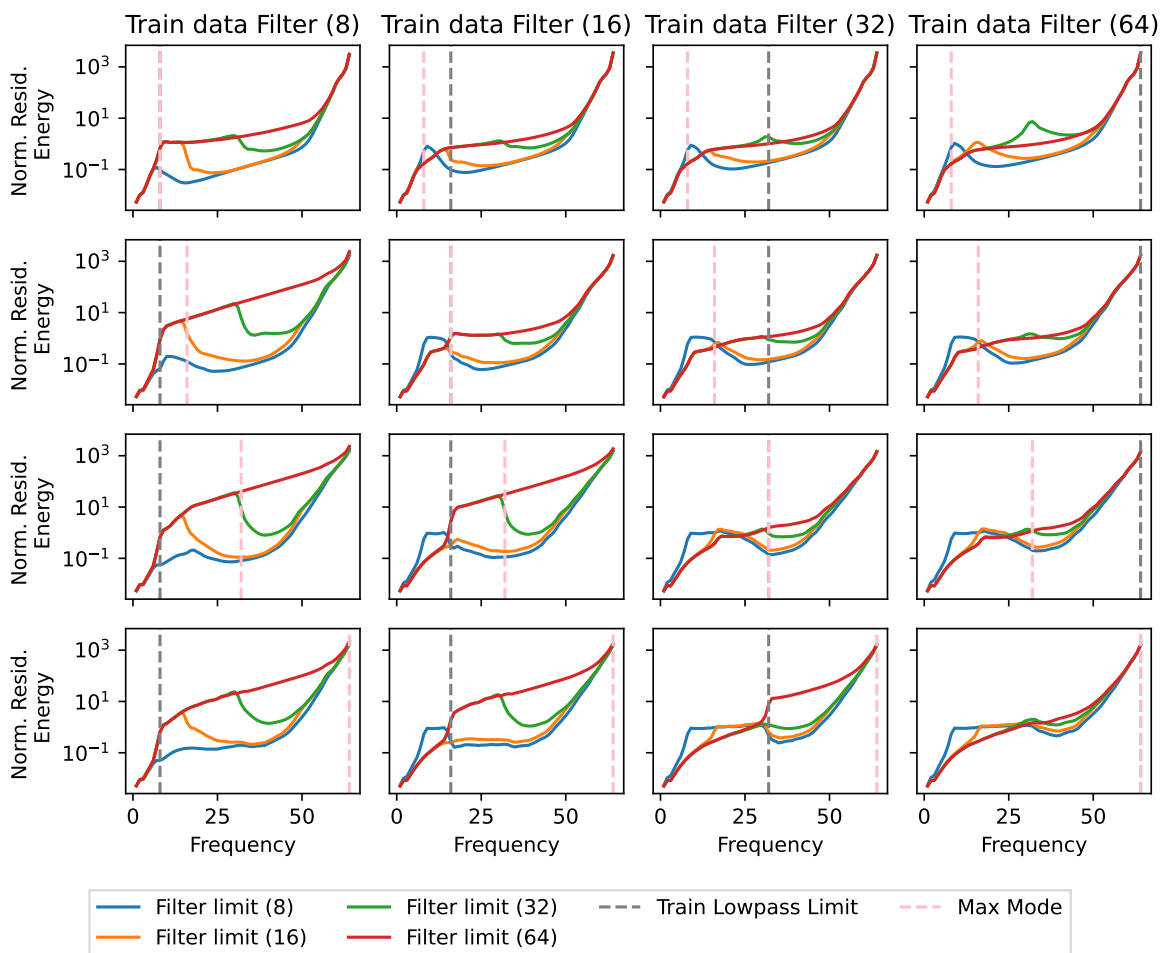


Figure 33: **Information Extrapolation.** Sixteen FNOs trained on Darcy data of resolution 128 (constant sampling rate) and low-pass filtered with limits  $\{8, 16, 32, 64\}$  (varying frequency information) from left to right, and top to bottom with max modes  $m \in \{8, 16, 32, 64\}$ . We test if each model can generalize to data with varying frequency information. Visualizing the spectrum of the normalized residuals across test data. Notice that the residual spectra (error) increases substantially in the high frequencies. Lower residual energy at all wave numbers is better. We observe that across all variation in  $m$ , the models assign high energy in the high-frequencies.